Supplementary Information for

Influence of ambient and endogenous H_2O_2 on reactive oxygen species concentrations and OH radical production in the respiratory tract

Eleni Dovrou[a,£,*], Steven Lelieveld[a], Ashmi Mishra[a], Ulrich Pöschl[a], Thomas Berkemeier[a*]

[a]Multiphase Chemistry Department, Max Planck Institute for Chemistry, Mainz 55128, Germany

[£]Now at: Institute of Chemical Engineering Sciences, Foundation for Research and Technology Hellas, Patra 26504, Greece

*Corresponding authors. Email: dovrouel@gmail.com, t.berkemeier@mpic.de

Supplementary Text

Section S1: Typical ambient and endogenous H_2O_2 concentrations

Gas-phase H_2O_2 is mainly produced via dismutation of the hydroperoxyl radical ($HO_2^{\bullet}$), which is formed by atmospheric photochemical processes. $HO_2^{\bullet}$is generated by the photolysis of formaldehyde and by reactions between hydroxyl radicals ($^{\bullet}OH$) and hydrocarbons. The formation of $^{\bullet}OH$ is triggered by photolysis of ozone, producing molecular and atomic oxygen, with the latter reacting with water vapor yielding $^{\bullet}OH$. Subsequently, $^{\bullet}OH$ reacts with hydrocarbons acting as a final source of $HO_2^{\bullet}$and H_2O_2. Anthropogenic sources, such as biomass burning, fire plumes, combustion facilities and vehicle exhausts yield both $HO_2^{\bullet}$and formaldehyde, contributing to H_2O_2 formation. An important source of high concentrations of H_2O_2 is thunderstorms, which produce H_2O_2 via electrical discharges during high electric field conditions. Thus, gas-phase H_2O_2 is continuously produced in the atmosphere via both natural and anthropogenic sources and constitutes the most abundant peroxide.[1,2]

In urban areas, typical ambient H_2O_2 levels are 0.5-1.5 ppb , while higher levels ≥2 ppb have been reported under polluted conditions in both urban and rural areas (Table S5).[3–7] Urban regions are typically characterized by elevated $^{\bullet}NO_x$ levels compared to rural areas, which, due to higher consumption of HO_2, may in some cases limit H_2O_2 production.

H_2O_2 has been investigated previously for its potential to trigger oxidative stress in the lung.[8–18] The chemical stability of H_2O_2 allows it to permeate biomembranes.[19] It is also produced endogenously via cellular sources. Cellular enzymes such as NADPH oxidase produce H_2O_2 via superoxide, which is subsequently converted to H_2O_2.[20–23] Cellular levels of H_2O_2 typically range from 1 to 100 nM.[12] Under oxidative signaling events, H_2O_2 levels reach up to 500-700 nM.[8,11] At high H_2O_2 levels, the cell can go into a state of oxidative stress, which can lead to inflammatory signaling and cell death.[12] H_2O_2 is also observed in blood with concentrations ranging from 0.8 to 6 μM for healthy individuals; individuals with diabetes or other health conditions can have H_2O_2 levels of 10-82 μM in their blood.[16,21,24,25] Measuring the H_2O_2 concentration in the ELF is challenging due to the difficulty in extracting lung lining fluid from a living organism.

Section S2: Kinetic multi-layer model

We investigate the effects and interactions of ambient and endogenous H_2O_2 and other air pollutants in the epithelial lining fluid (ELF) using a multiphase kinetic model, which builds on an existing kinetic modeling framework[26,27] and describe chemical mechanisms and transport of reactive oxygen species (ROS) influencing oxidative stress. In the model, the respiratory tract is divided into: (a) the gas phase of the respiratory tract, (b) the surfactant layer, (c) the aqueous ELF, (d) a cellular layer, and (e) a blood layer.

The kinetic multi-layer model of surface and bulk chemistry in the epithelial lining fluid (KM-SUB-ELF) described by Lakey et al.[26] and Lelieveld et al.[27] was extended to simulate the production rate and concentration of ROS in the ELF considering effects of underlying cells and blood vessels. The newly developed model (KM-SUB-ELF 2.0) treats inhalation and exhalation from and to the ambient gas phase, adsorption and desorption to and from the ELF, diffusion in the ELF, mass transport between the ELF, cells and blood, as well as 131 chemical reactions are represented in the model. The model considers particulate pollution from fine particulate matter smaller than 2.5 μm (PM2.5) and gas-phase pollution from $^{\bullet}NO_2$, O_3, and H_2O_2. The model generates a system of ordinary differential equations, which is solved using the stiff differential equation solver *ode23tb* in Matlab, and calculates the evolution of reactant concentrations over time. An explicit Jacobian matrix is provided to aid in computation. Model parameters are listed in Tables S1-S4.

The surfactant layer consists of a surfactant lipid, 1-palmitoyl-2-oleoyl-*sn*-glycerol (POG), a surfactant protein ($SP\text{-}B_{1\text{-}25}$), and the antioxidant α-tocopherol (α-Toc), following Lelieveld et al. [27]. Chemical reactions of POG and $SP\text{-}B_{1\text{-}25}$ with $^{\bullet}OH$ and O_3 occur in this compartment. The ozonolysis of POG yields Criegee intermediates, which are assumed to hydrolyze to H_2O_2 according to reaction R1 with an experimentally-determined yield of 0.17.[27] Diffusion of ROS between the surfactant layer and the ELF can increase ROS concentrations in the ELF.

$$\mathrm{POG} + \mathrm{O_3} \rightarrow \mathrm{HCHO} + (0.17)\mathrm{H_2O_2} \qquad 1.66 \times 10^{-16}\ \mathrm{cm^3\ s^{-1}} \qquad (1)$$

The low molecular mass antioxidants ascorbate (Asc), glutathione (GSH), uric acid (UA), and α-Toc) are included in the model. In addition, the model considers three quinones as part of PM2.5, phenanthrenequinone, 1,2-naphthoquinone and 1,4-naphthoquinone, and their reaction with oxygen, $HO_2^{\bullet}$, and Asc. Ambient and endogenous contributions, Fenton chemistry involving iron and copper, as well as HO_x ($\equiv ^{\bullet}OH$, $HO_2^{\bullet}$) chemistry are main pathways leading to formation and consumption of H_2O_2 and thus ROS. The rate coefficients follow the work of Lakey et al.[26]. All reactions included in the model are listed in Table S1. Partitioning from gas phase into the surfactant layer is calculated according to Henry's law for aqueous solutions. Accordingly, equal partitioning is assumed between surfactant and aqueous ELF layer for all volatile species.

The composition of PM2.5 in the atmosphere varies strongly depending on location, source, season, weather, and time of day. We use a standardized PM2.5 composition that was established previously using the median mass fractions of redox-active PM2.5 constituents from a large set of atmospheric field measurements.[27] The mass fractions are 3.1×10^{-4} for copper, 8.1×10^{-3} for iron, 1.6×10^{-5} for quinones, and 0.33 for secondary organic aerosol (SOA).

The most influential model parameters are varied for sensitivity analyses in this study (Figs. 2 and 3, Figs. S1-S7). However, if not noted otherwise, these parameters are kept at their default values. The default effective membrane permeability of H_2O_2 is 1×10^{-5} cm s^{-1}, the default blood

concentration of H_2O_2 is 5 μM, the default ambient concentration of H_2O_2 is 1 ppb, the default cellular production rate of H_2O_2 is 1×10^{14} cm^{-3} s^{-1}, and the default concentration of H_2O_2-scavenging enzymes in the cell layer is 10 μM (Table S4).

Section S3: Antioxidant concentrations and enzymatic reactions

In the model, the antioxidants Asc, GSH, and UA are present in the ELF at concentrations of 40 μM, 108 μM, and 200 μM, respectively.[26–29] α-Toc is considered to be in the surfactant layer with concentration of 200 μM.[27] In line with previous models, antioxidants are considered constant within the two-hour simulation time to prevent the significant changes in redox chemistry in the unlikely event of full antioxidant depletion.[27]

Enzymatic reactions are considered within ELF and cellular compartments. Superoxide dismutase (SOD) and catalase are included in ELF, while in cells, a range of H_2O_2-scavenging enzymes (peroxiredoxins, catalase, GSH peroxidase) are considered as outlined below and in Table S2. The reaction of SOD with $O_2^{\bullet-}$ results in the production of H_2O_2 and O_2, each with 50% yield.[27] Catalase has been experimentally determined to be the main defense of ELF against H_2O_2, following a two-step reaction mechanism.[30–32] In the first step H_2O_2 reacts with catalase forming a catalase-H_2O_2 complex, which, in the second step, reacts with another H_2O_2 molecule forming water and oxygen. In this work, the two steps are combined, producing water and oxygen with a 50% yield, respectively.

The catalytic activity of enzymes is typically reported in enzyme units (U), defined as the amount of enzyme required to catalyze one micromole of substrate per minute. In the substrate-limited regime, the enzyme concentration can be calculated as the ratio of the catalytic activity v_{max}, given in U mL^{-1}, and the catalytic constant, k_{cat}.

$$[\text{enzyme}] = \frac{v_{\max}}{k_{\text{cat}}} \tag{8}$$

For SOD, k_{cat} has been reported between 10^5-10^6 s^{-1} and v_{max} at 36.8±2.0 U mL^{-1}.[27,30,33,34] Using Eq. 8, the SOD concentration can be estimated between 0.61 and 6.1 nM. Similarly, k_{cat} for catalase is reported in the range of 3×10^6-4×10^7 s^{-1} with a v_{max} of 3.7±0.6 U mL^{-1}, resulting in an estimated catalase concentration range of 1.6-16 pM.[30,35] From these concentration ranges, 1 nM of SOD and 5 pM of catalase are chosen as an order of magnitude estimate, respectively, following the work of Lelieveld et al.[27]. In the cellular layer, the catalytic activity of catalase is reported to be an order of magnitude higher compared to ELF, which equates to 50 pM.[36,37] In contrast, peroxiredoxins are thiol proteins that are present in the cells at much higher concentrations of tens of micromolar.[38] Hence, peroxiredoxins are likely the predominant sink of H_2O_2 in lung cells. Thus, for simplicity, we choose a conservative estimate of 10 μM for the sum of all H_2O_2-scavenging enzymes in this work, and assume a common reaction rate of 3.3×10^{-14} cm^3 s^{-1} for the enzymes.[38] Note that H_2O_2 is scavenged only by the reduced forms of peroxiredoxins, yielding peroxiredoxins in an oxidized form. The reduced form must be regenerated in a NADPH-dependent reaction.[39] Here, we assume that the concentration of the reduced form of peroxiredoxins is constant during the calculation.

Section S4: Production of H_2O_2 in the cellular layer

Respiratory cells are known ROS producers, among them type II alveolar cells and endothelial cells. Type II alveolar cells constitute about 4 % of the alveolar surface area and 10-15 % of all

lung cells.[40] Kinnula et al.[41] find a production rate of 0.7 nmol H_2O_2 min^{-1} mg $protein^{-1}$ for type II alveolar cells and 0.06 nmol H_2O_2 min^{-1} mg $protein^{-1}$ for endothelial cells. Piotrowski et al.[42] find a baseline production of type II alveolar cells of 0.15 nmol H_2O_2 min^{-1} mg $protein^{-1}$. We estimate from literature that the protein mass density is in the range of 150 – 300 mg cm^{-3}.[43] Using these numbers, we can derive a best estimate for the cellular H_2O_2 production rate in the range of 2×10^{13} – 5×10^{14} cm^{-3} s^{-1} as detailed below. Note, however, that these measurements stem from *in vitro* experiments using rat alveolar cells and can only be regarded as order of magnitude estimates for the human lung. We thus choose a central value of 1×10^{14} cm^{-3} s^{-1} from this range for the calculations in this study.

Upper Estimate - 15 % of cells are type II alveolar cells (0.7 nmol mg $protein^{-1}$ min^{-1}) and the rest behave like endothelial cells (0.06 nmol mg $protein^{-1}$ min^{-1}) at a protein mass density of 300 mg cm^{-3}

$$(0.15 \cdot 0.7\ \text{nmol mg}^{-1}\ \text{min}^{-1} + 0.85 \cdot 0.06\ \text{nmol mg}^{-1}\ \text{min}^{-1}) \cdot 300\ \text{mg cm}^{-3} \cdot 6.022 \cdot 10^{23}\ \text{mol}^{-1} \cdot \frac{1}{60}\text{min s}^{-1} \approx 5 \cdot 10^{14}\ \text{cm}^{-3}\ \text{s}^{-1}$$

Lower Estimate - 10 % of cells are type II cells (0.15 nmol mg $protein^{-1}$ min^{-1}) at a protein mass density of 150 mg cm^{-3} and the remaining cells do not produce significant amounts of H_2O_2

$$(0.1 \cdot 0.15\ \text{nmol mg}^{-1}\ \text{min}^{-1}) \cdot 150\ \text{mg cm}^{-3} \cdot 6.022 \cdot 10^{23}\ \text{mol}^{-1} \cdot \frac{1}{60}\text{min s}^{-1} \approx 2 \cdot 10^{13}\ \text{cm}^{-3}\ \text{s}^{-1}$$

Section S5: Secondary Organic Aerosol (SOA)

Secondary organic aerosol (SOA) is a major component of ambient PM2.5[44,45] and contains highly oxidized organic compounds such as organic (hydro)peroxides.[46] These peroxides may be labile and decay with a short half-life[47] or follow a similar chemistry to H_2O_2 by forming $^{\bullet}OH$ radicals in reactions with transition metals and water.[48] SOA has been shown to produce superoxide and H_2O_2 in aqueous solution and to contribute to the oxidative potential and cytotoxicity of PM2.5.[49–52]

SOA may contribute to $^{\bullet}OH$ production in an iron-dependent and an iron-independent process.[47,48] Following the work of Tong et al. [48] and Lakey et al. [26], we consider a relative $^{\bullet}OH$ yield from SOA of 1% within the 2-hour calculation window. However, expanding the parameterization in Lakey et al.,[26] we attribute a tenth, i.e. 0.1 % of SOA, to iron-independent SOA sources (Fig. S8), which is in line with the observations in Tong et al.[48].

Note that the contribution of SOA to $^{\bullet}OH$ production in epithelial lining fluid is not well established. Interpreting experimental results that contain a multitude of chemical components is very challenging. Furthermore, experiments are often performed using electron paramagnetic resonance (EPR) spectroscopy and radical detection with spin trapping agents. These techniques are affected by radical-spin trap-adduct half-lives and yields, which further hamper experimental interpretation. As an example, recent studies find differences in the type and amount of radical species formed in pure water or in surrogate lung fluid (SLF).[48,51,53,54] While $^{\bullet}OH$ and superoxide have been observed in experiments performed in pure water,[48,53] $R^{\bullet}$ radicals have been found as the major product in SLF.[51,54] These observations indicate either a different decomposition mechanism of SOA, or altered radical-spin trap-adduct half-lives and yields under the different

experimental conditions. It remains open whether •OH is formed initially, but reacts with other SLF constituents before reaction with the spin trapping agent. Furthermore, organic peroxides inhaled through SOA may also be scavenged by enzymes such as peroxiredoxins and peroxidases before significant conversion to •OH occurs. Comprehensive experimental and modelling analyses are required to unravel the exact mechanism and extent of radical formation from SOA in epithelial lining fluid. However, this is out of the scope of the present work. For these reasons, the contribution of SOA to •OH production in this work may constitute an upper estimate.

Section S6: H_2O_2 and •OH source apportionment in ELF

In this study, the source apportionment of H_2O_2 in the ELF could not be achieved with traditional flux analyses, i.e. comparing chemical and diffusion fluxes, due to the inherit coupling of chemical reaction and diffusion in multiple compartments. Instead, we performed a sensitivity analysis and compared five scenarios (endogenous transport of H_2O_2, inhalation of ambient H_2O_2, $^{\bullet}NO_2$, O_3, and PM2.5), in which only a single source was present in the model at a time, to the scenario with all sources. For instance, to estimate the H_2O_2 concentration attributed to endogenous transport of H_2O_2, the sources from ambient H_2O_2, O_3, NO_2 and PM2.5 were turned off. We followed the same approach for each of the five sources. Note that this approach was only possible because non-linear effects were almost non-existent, i.e. the total H_2O_2 concentration was very close to the sum of the H_2O_2 generated in each single-source scenario. Thus, dividing the H_2O_2 concentration in each single-source scenario over the H_2O_2 concentration considering all sources gives a good approximation of the apportionment of sources.

For source apportionment of the hydroxyl radical (•OH), a traditional flux analysis could be performed due to negligible diffusion of the reactive radical across compartment boundaries. The production of •OH is mainly attributed to Fenton(-like) reactions of H_2O_2 and SOA with iron in the model.

The H_2O_2 consumption by enzymes in the cell layer affects the source apportionment of •OH production and H_2O_2 concentration (Fig. S7b). Increase of the enzyme concentration leads to a decrease in contribution of Fenton chemistry (H_2O_2/Fe) to •OH production, shifting the contribution towards the Fenton-like reactions involving SOA (SOA/Fe). Figure S4b shows a stronger influence of endogenous H_2O_2 in the H_2O_2 concentration in the ELF at low enzyme concentrations. The endogenous and gas-phase H_2O_2 contributions converge with increasing enzyme availability.

Section S7: Discussion of model sensitivity and limitations

The model presented in this work, KM-SUB-ELF 2.0, describes chemical mechanisms and transport of ROS within the respiratory tract, aiming to investigate the influence of ambient and endogenous H_2O_2 as well as main air pollutants in ROS production. Due to the complexity of the respiratory tract, KM-SUB-ELF 2.0 outlines the essential processes to provide a first estimate on evaluating the parameters influencing ROS production. A key model parameter is the effective membrane permeability of H_2O_2 (μ_{eff}. Figures 2a and S1a show the concentrations of H_2O_2 in all model compartments as a function of μ_{eff}. The concentrations in atmosphere and blood in the model are not affected, but the ELF and cellular concentrations are strongly influenced by μ_{eff}. The reported range of cellular H_2O_2 (1-10 nM) constrains this important model parameter. The value of μ_{eff} also affects the •OH source (Fig. S7a): at the best guess value for μ_{eff}, •OH production is

mainly due to Fenton chemistry of peroxides contained in SOA, while at very high or very low μ_{eff}, Fenton chemistry of H_2O_2 is the dominant $^{\bullet}OH$ source.

It is important to note that the $^{\bullet}OH$ yield from SOA is a challenging topic, requiring further investigation and thus contributing to the uncertainty of the calculations. This topic is discussed in detail in Sect. S5, but a more in-depth investigation is out of the scope of this study.

Another important parameter influencing the ROS levels in the respiratory tract is the cellular concentration of H_2O_2-scavenging enzymes. Figure S1b shows a linear dependence of H_2O_2 concentration in the cells and a similarly strong dependence of H_2O_2 concentration in the LLF, which levels off towards very high enzyme concentrations.

The concentration of PM2.5 determines the production of $^{\bullet}OH$ in the ELF, as shown in Figure 3B and D. The concentrations of H_2O_2 in ELF and respiratory tract gas phase, however, are not affected by PM2.5 concentrations (Figs. S1c, S3c). PM2.5 becomes a significant source of H_2O_2 only at the highest concentrations investigated in this study (1000 µg/m3; Fig. S4c), which are exceedingly high even for the most polluted cities on Earth.

We finally note that the biological mechanisms contributing to ROS production and consumption are strongly simplified in the model. Future work is needed to include biological sources of superoxide and their stimulation with PM2.5.[55] The model structure of the respiratory tract could be further subdivided, for example into extrathoracic, bronchial, and alveolar space (Fig. S9), which likely experience different concentrations of deposited PM2.5 and inhaled water-soluble trace gases such as H_2O_2, NO_2 and O_3. Preliminary calculations separating upper and lower respiratory tract show that between 10-90 % of ambient gas-phase H_2O_2 will be consumed in the extrathoracic space (nasal cavity to trachea) alone, depending on factors such as geometry, ELF volume, H_2O_2-scavenging enzyme concentrations, and membrane permeability in the upper respiratory tract. The exhaled H_2O_2 concentrations in this early test simulation were strongly increased, due to a higher saturation of the extrathoracic ELF with H_2O_2, coming much closer to values reported for exhaled breath condensate. We expect that the upgraded model structure and inclusion of macrophages as additional endogenous ROS sources will reconcile the agreement with these measurements, and decrease the importance of ambient H_2O_2 for the deep lung. However, this model upgrade is still in development, outside the scope of this work, and will be addressed in future publications. Nevertheless, this work provides important insights in the evaluation of toxicity of the main air pollutants and the effect of endogenous processes to ROS levels in the respiratory tract.

Section S8: Contribution of ambient and endogenous H_2O_2 to ROS in the ELF

In the model KM-SUB-ELF 2.0, the concentration of H_2O_2 in ELF can be either determined by transport of endogenous H_2O_2 (endogenous H_2O_2 regime), inhalation of ambient H_2O_2 (ambient H_2O_2 regime) or both (transition regime). Which regime is active depends on the effective membrane permeability μ_{eff}, with the ambient H_2O_2 regime dominating the H_2O_2 concentration in ELF when $\mu_{eff} < 1 \cdot 10^{-5}$ cm s^{-1}, while the endogenous H_2O_2 regime dominates the H_2O_2 concentration in the ELF when $\mu_{eff} > 1 \times 10^{-5}$ cm s^{-1} (Figs. 2 and S3). At 1×10^{-5} cm s^{-1}, the best guess for membrane permeability in this study, we observe a transition between both regimes. Figure S5 illustrates the regimes of H_2O_2 supply: in the ambient-H_2O_2 regime, only changes in ambient H_2O_2 concentrations change the H_2O_2 concentrations in the ELF. Likewise, in the endogenous H_2O_2 regime, only changes in blood H_2O_2 concentrations change the H_2O_2

concentrations in the ELF. In the transition range between both regimes, both concentrations are important. Note that, while membrane permeability of H_2O_2 affects the regime of H_2O_2 supply, $^{\bullet}OH$ production in the ELF is dominated by PM2.5 constituents regardless of μ_{eff} in the model. Note also that additional endogenous sources of ROS, such as superoxide production by macrophages in the ELF or a larger production rate of H_2O_2 by epithelial cells, may tip the scales fully in favor of endogenous sources of H_2O_2.

Supplementary Figures

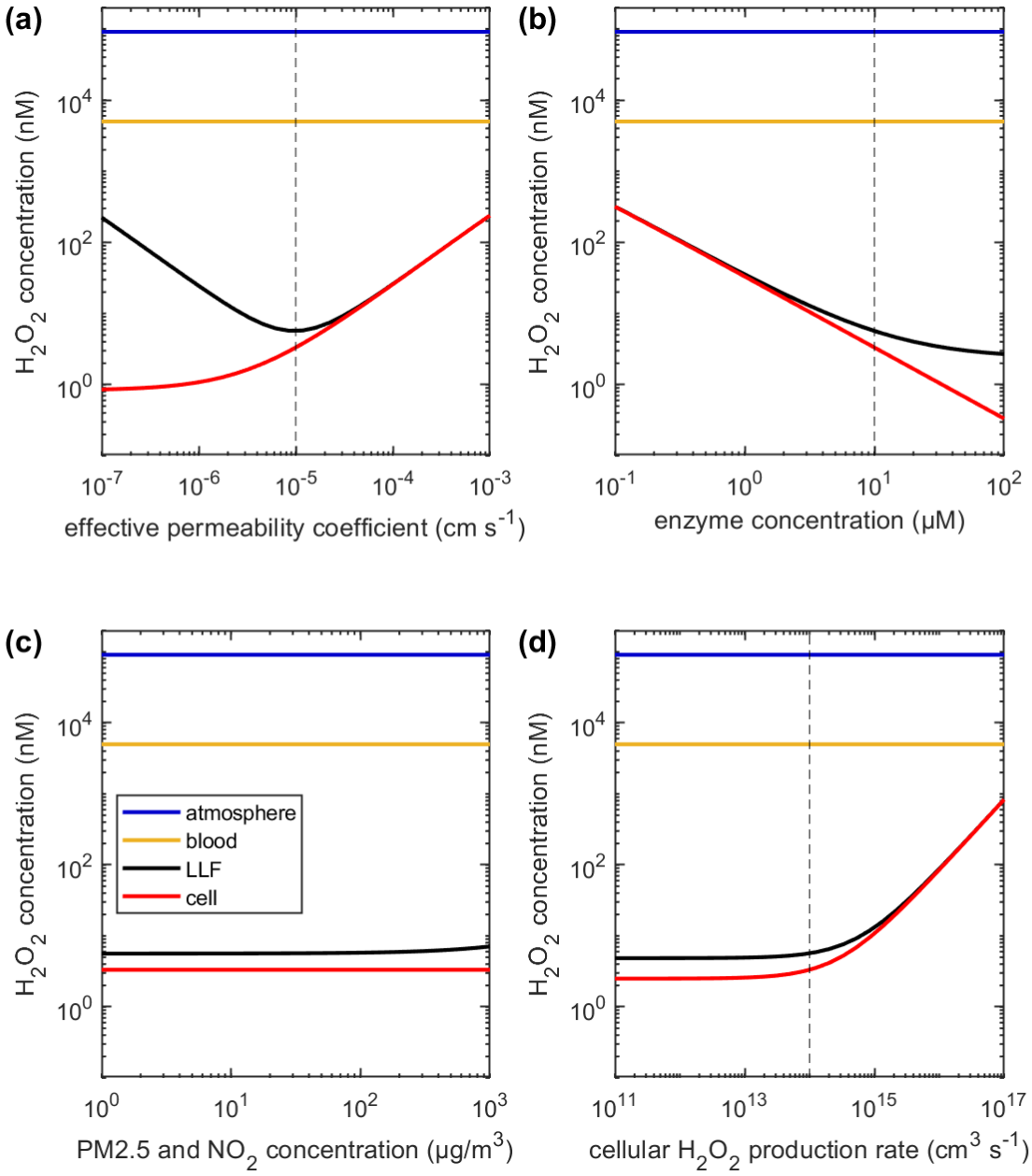

Fig. S1. H_2O_2 concentrations in respiratory tract compartments. H_2O_2 concentration in blood (red line), epithelial lining fluid (ELF; black line), and cells (orange line) as a function of various model parameters: (a) effective membrane permeability coefficient of H_2O_2, (b) H_2O_2-scavenging enzyme concentration in cells, (c) ambient PM2.5 and NO_2 concentration, and (d) cellular H_2O_2 production rate in a standard pollution scenario (PM2.5=30 μg m^{-3}, NO2=30 μg m-3, O3=30 ppb, H_2O_2=1 ppb) unless otherwise indicated. Effective permeability and enzyme concentration are the parameters with the strongest sensitivity, while cellular H_2O_2 production rate only becomes sensitive at large values. The parameters used in the standard scenario in this study are marked with a vertical dashed line.

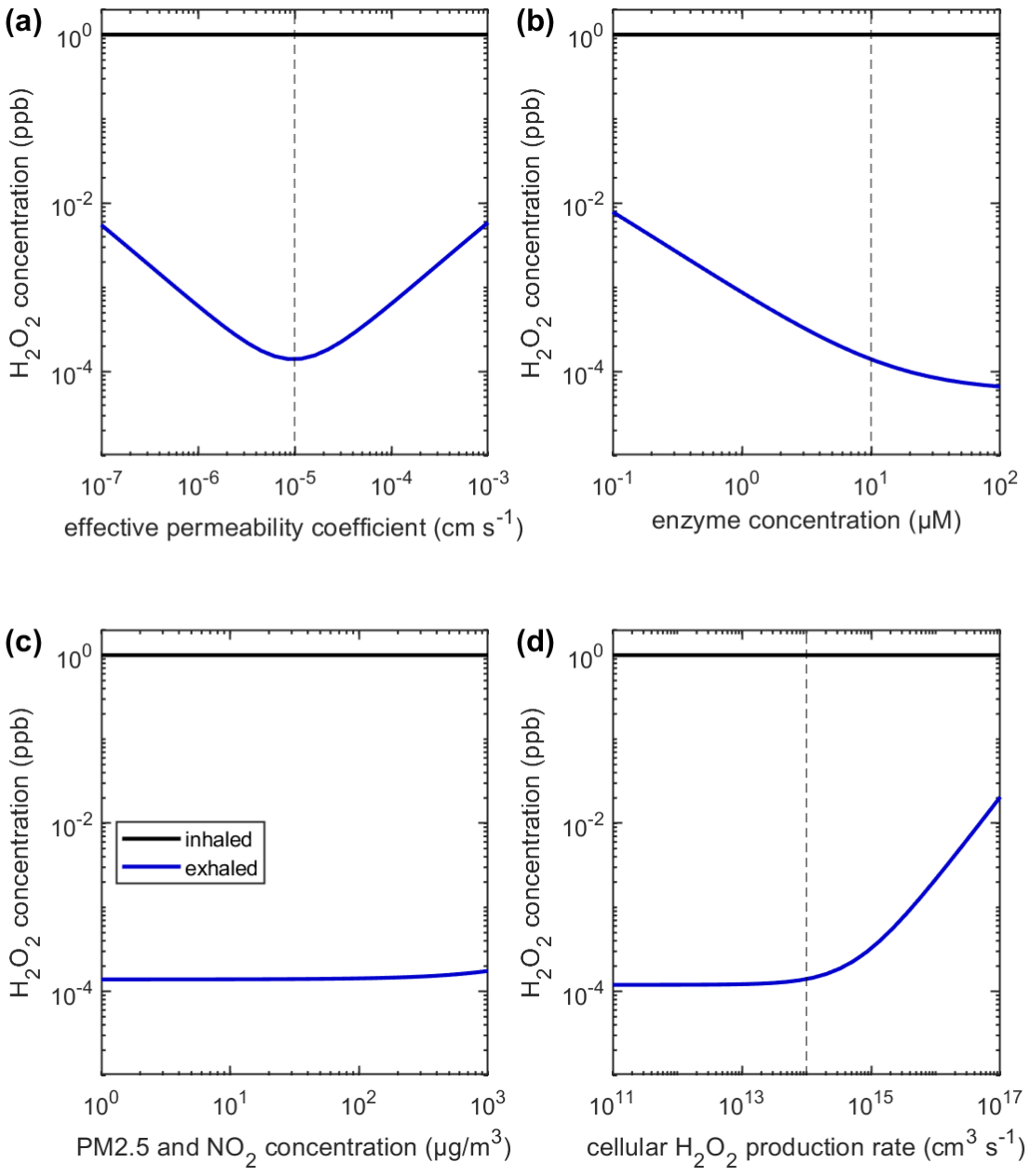

Fig. S2. Comparison of inhaled and exhaled H_2O_2 concentrations. Inhaled and exhaled H_2O_2 concentrations as a function of various model parameters: (a) effective membrane permeability coefficient of H_2O_2, (b) H_2O_2-scavenging enzyme concentration in cells, (c) ambient PM2.5 and NO_2 concentration, and (d) cellular H_2O_2 production rate in a standard pollution scenario (PM2.5=30 μg m^{-3}, NO_2=30 μg m^{-3}, O_3=30 ppb, H_2O_2=1 ppb) unless otherwise indicated. Inhaled H_2O_2 concentrations are always larger than exhaled concentrations. The parameters used in the standard scenario in this study are marked with a vertical dashed line.

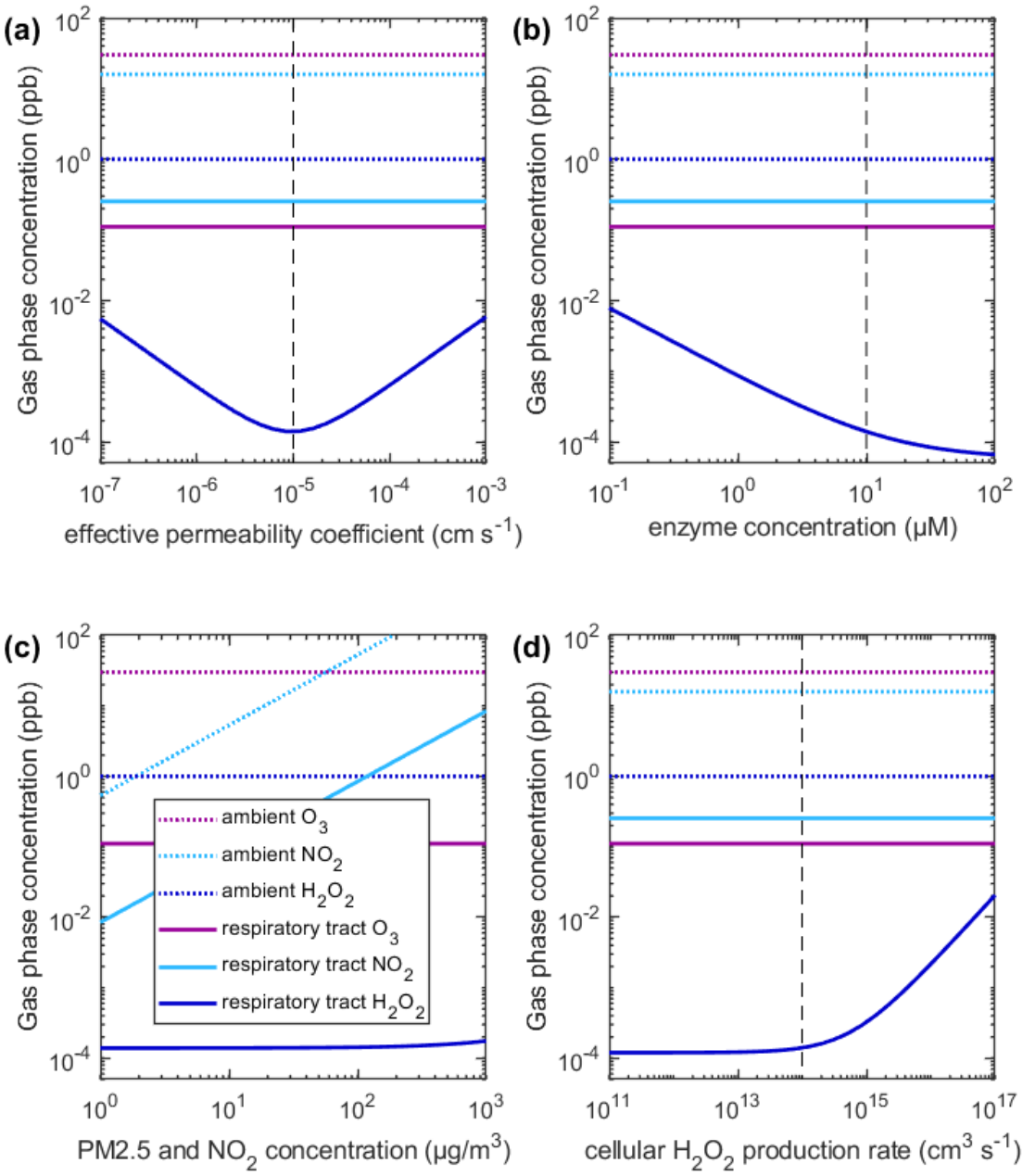

Fig. S3. Comparison of ambient and respiratory tract gas-phase concentrations. The ambient (dotted lines) and respiratory tract (solid lines) gas-phase concentrations of H_2O_2 (blue), O_3 (purple), and NO_2 (black line) as a function of various model parameters: (a) effective membrane permeability coefficient of H_2O_2, (b) H_2O_2-scavenging enzyme concentration in cells, (c) ambient PM2.5 and NO_2 concentration, and (d) cellular H_2O_2 production rate in a standard pollution scenario (PM2.5=30 μg m^{-3}, NO_2=30 μg m^{-3}, O_3=30 ppb, H_2O_2=1 ppb) unless otherwise indicated. All respiratory tract / exhaled concentrations are significantly below their ambient / inhaled concentrations due to reactive uptake to the epithelial lining fluid. The parameters used in the standard scenario in this study are marked with a vertical dashed line.

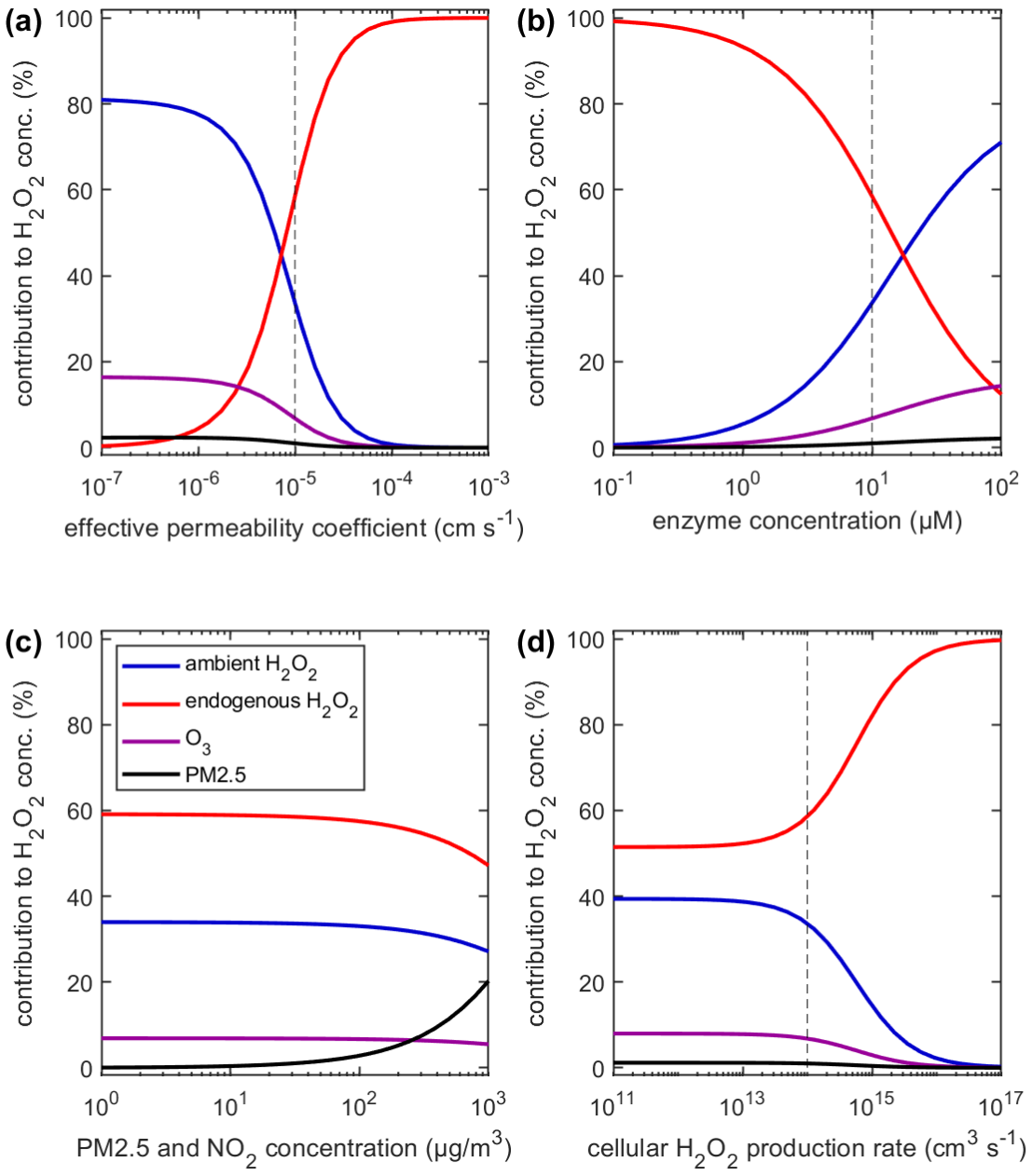

Fig. S4. Source apportionment of H_2O_2 sources in the ELF. The contribution of ambient H_2O_2 (blue line), endogenous transport of H_2O_2 (red line), ozone (purple line), and PM2.5 (black line) as a function of various model parameters: (a) effective membrane permeability coefficient of H_2O_2, (b) H_2O_2-scavenging enzyme concentration in cells, (c) ambient PM2.5 concentration, and (d) cellular H_2O_2 production rate in a standard pollution scenario (PM2.5=30 μg m^{-3}, NO_2=30 μg m^{-3}, O_3=30 ppb, H_2O_2=1 ppb) unless otherwise indicated. The dominant sources are ambient H_2O_2 and endogenous transport of H_2O_2, but the contributions are strongly influenced by the effective membrane permeability and H_2O_2-scavenging enzyme concentration in cells. The parameters used in the standard scenario in this study are marked with a vertical dashed line.

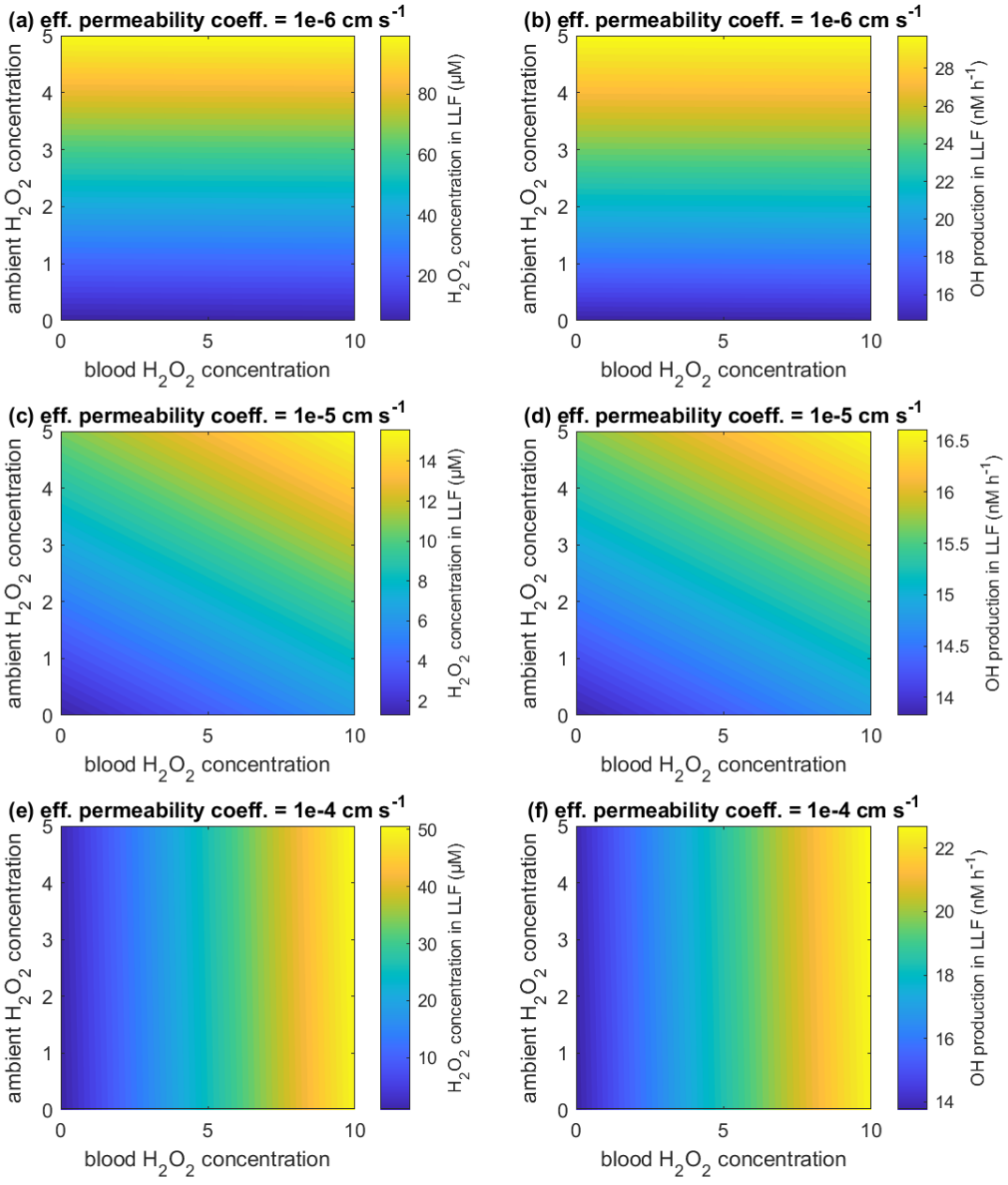

Fig. S5. Comparison of the influence of inhalation of ambient H_2O_2 and transport of endogenous H_2O_2. H_2O_2 concentration (panels a, c, e) and $^{\bullet}OH$ production (panels b, d, f) in ELF are displayed as a function of ambient and blood H_2O_2 concentrations and for three different values of the effective membrane permeability coefficient of H_2O_2. A higher effective membrane permeability of H_2O_2 enhances the influence of endogenous transport of H_2O_2, which is evident from the increasingly vertical contour lines. While the system is clearly in the *ambient-H_2O_2 regime* in panels (a) and (b), it is fully in the *endogenous-H_2O_2 regime* in panels (e) and (f).

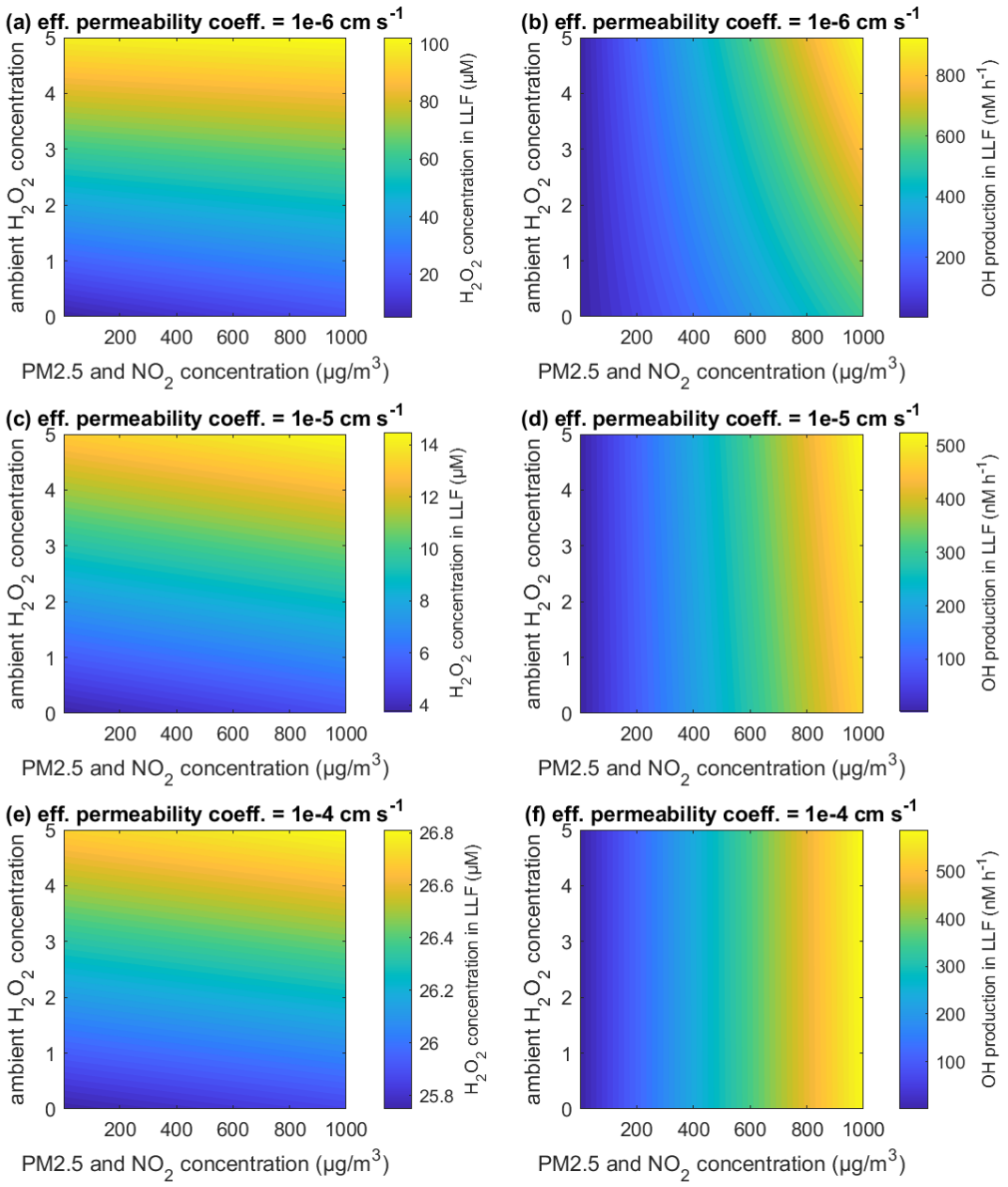

Fig. S6. Comparison of the influence of inhalation of ambient H_2O_2 and PM2.5 concentration. H_2O_2 concentration (panels a, c, e) and $^{\bullet}OH$ production (panels b, d, f) in ELF as a function of ambient and PM2.5 concentrations and for three different values of the effective membrane permeability coefficient of H_2O_2. The value of the effective permeability coefficient has only very little effect on the general result that $^{\bullet}OH$ production is dominated by PM2.5 concentrations, while H_2O_2 concentration is hardly affected by PM2.5 concentrations.

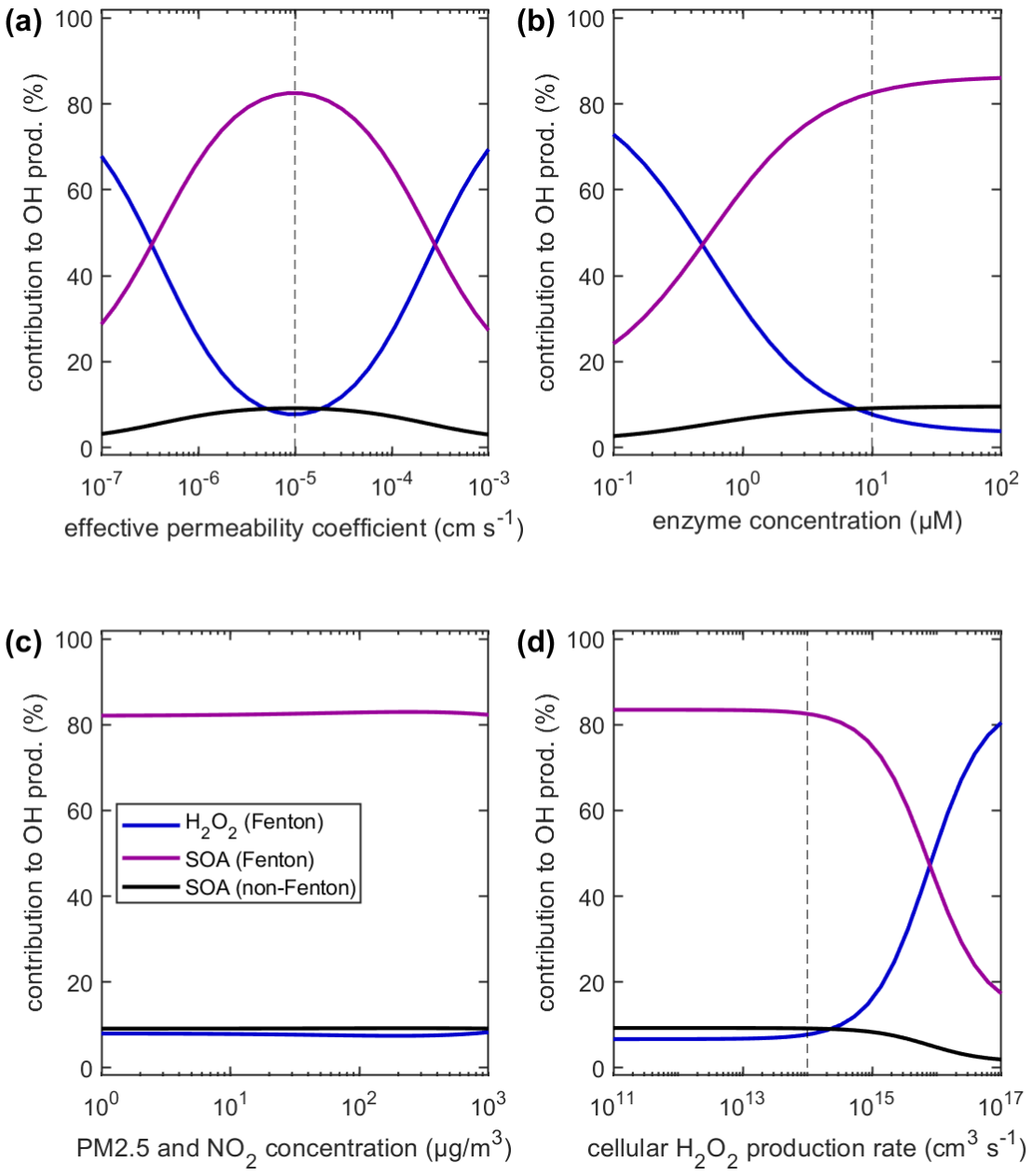

Fig. S7. Source apportionment of ˙OH sources in the ELF. The contribution of Fenton chemistry of H_2O_2 (blue line), Fenton chemistry of SOA (purple line), and non-Fenton chemistry of SOA (black line) as a function of various model parameters: (a) effective membrane permeability coefficient of H_2O_2, (b) H_2O_2-scavenging enzyme concentration in cells, (c) ambient PM2.5 concentration, and (d) cellular H_2O_2 production rate in a standard pollution scenario (PM2.5=30 μg m^{-3}, NO_2=30 μg m^{-3}, O_3=30 ppb, H_2O_2=1 ppb) unless otherwise indicated. The dominant sources are Fenton chemistry of H_2O_2 and SOA, but the contributions are strongly influenced by the effective membrane permeability and H_2O_2-scavenging enzyme concentration in cells. The parameters used in the standard scenario in this study are marked with a vertical dashed line.

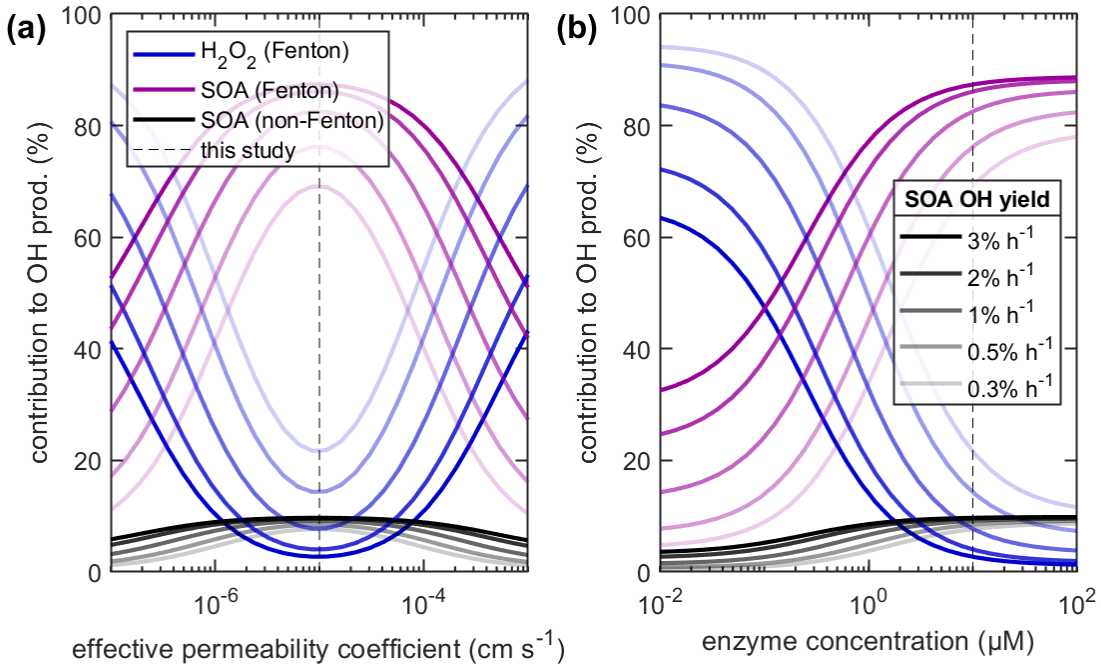

Fig. S8. Source apportionment of ˙OH sources in the ELF as a function of aqueous SOA chemistry. Effect of effective permeability and H_2O_2-scavenging enzyme concentration in cells on ˙OH production. The contribution of Fenton chemistry of H_2O_2 (blue line), Fenton chemistry of SOA (purple line), and non-Fenton chemistry of SOA (black line) as a function of various model parameters: (a) effective membrane permeability coefficient of H_2O_2, (b) H_2O_2-scavenging enzyme concentration in cells. The results are given for a range of ˙OH yield of SOA (0.3-3 % h^{-1}).

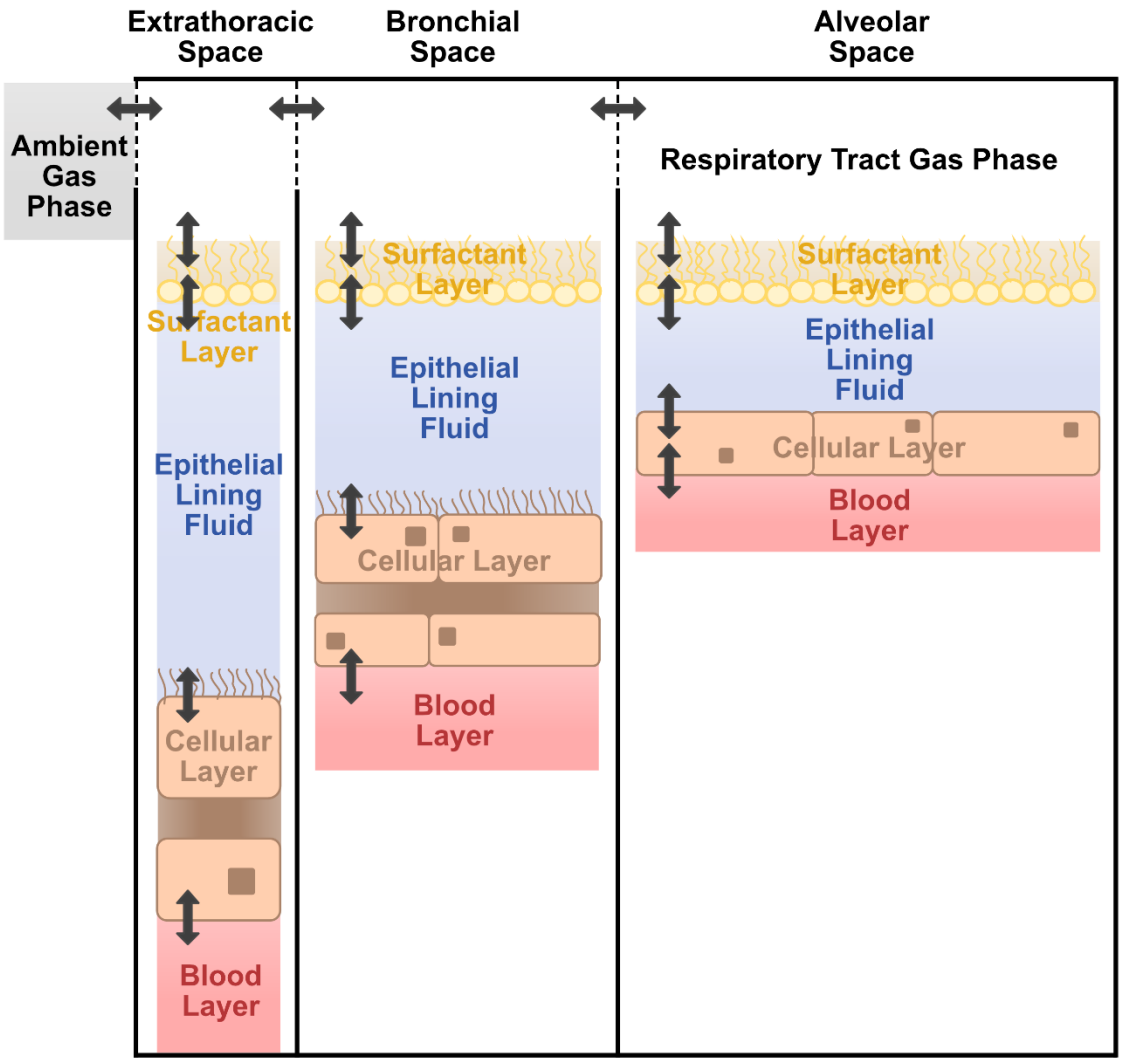

Fig. S9. Proposed model structure for follow-up study. To improve the model, we suggest a sub-division of the respiratory tract. Shown here is a schematic representation of the respiratory tract in three parts: extrathoracic, bronchial and alveolar space. Geometry of those three spaces will be different with the extrathoracic space having the largest layer thicknesses but least overall surface area, and the alveolar space the smallest layer thicknesses but largest surface area, respectively (schematic not to scale). The gas-phase compartments will be connected through a fast flux according to the breathing rate.

Supplementary Tables

Table S1. Chemical reactions included in the model.

Reaction	Compartment	Rate constant	Unit	Reference	#
$^{\bullet}NO + O_3 \rightarrow {}^{\bullet}NO_2 + O_2$	Gas	$2.05 \cdot 10^{-14}$	$cm^3\ s^{-1}$	56,57	1
$^{\bullet}NO_2 + O_3 \rightarrow {}^{\bullet}NO_3 + O_2$	Gas	$4.85 \cdot 10^{-17}$	$cm^3\ s^{-1}$	56,57	2
$^{\bullet}NO + {}^{\bullet}NO \xrightarrow{O_2} {}^{\bullet}NO_2 + {}^{\bullet}NO_2$	Gas	$8.93 \cdot 10^{-20}$	$cm^3\ s^{-1}$	56,57	3
$^{\bullet}NO + {}^{\bullet}NO_3 \rightarrow {}^{\bullet}NO_2 + {}^{\bullet}NO_2$	Gas	$2.57 \cdot 10^{-11}$	$cm^3\ s^{-1}$	56,57	4
$^{\bullet}NO_2 + {}^{\bullet}NO_3 \rightarrow {}^{\bullet}NO + {}^{\bullet}NO_2 + O_2$	Gas	$7.73 \cdot 10^{-16}$	$cm^3\ s^{-1}$	56,57	5
$^{\bullet}NO_2 + {}^{\bullet}NO_3 \rightarrow N_2O_5$	Gas	$1.21 \cdot 10^{-12}$	$cm^3\ s^{-1}$	56,57	6
$^{\bullet}OH + O_3 \rightarrow HO_2^{\bullet} + O_2$	Gas	$8.20 \cdot 10^{-14}$	$cm^3\ s^{-1}$	56,57	7
$^{\bullet}OH + H_2O_2 \rightarrow HO_2^{\bullet} + H_2O$	Gas	$1.73 \cdot 10^{-12}$	$cm^3\ s^{-1}$	56,57	8
$HO_2^{\bullet} + O_3 \rightarrow {}^{\bullet}OH + O_2 + O_2$	Gas	$8.24 \cdot 10^{-16}$	$cm^3\ s^{-1}$	56,57	9
$^{\bullet}OH + HO_2^{\bullet} \rightarrow H_2O + O_2$	Gas	$1.08 \cdot 10^{-10}$	$cm^3\ s^{-1}$	56,57	10
$HO_2^{\bullet} + HO_2^{\bullet} \rightarrow H_2O_2 + O_2$	Gas	$5.09 \cdot 10^{-12}$	$cm^3\ s^{-1}$	56,57	11
$HO_2^{\bullet} + HO_2^{\bullet} \rightarrow H_2O_2$	Gas	$3.50 \cdot 10^{-12}$	$cm^3\ s^{-1}$	56,57	12
$^{\bullet}OH + {}^{\bullet}NO \rightarrow HONO$	Gas	$8.91 \cdot 10^{-12}$	$cm^3\ s^{-1}$	56,57	13
$^{\bullet}OH + {}^{\bullet}NO_2 \rightarrow HNO_3$	Gas	$8.91 \cdot 10^{-12}$	$cm^3\ s^{-1}$	56,57	14
$^{\bullet}OH + NO_3^{\bullet} \rightarrow HO_2^{\bullet} + {}^{\bullet}NO_2$	Gas	$2.00 \cdot 10^{-11}$	$cm^3\ s^{-1}$	56,57	15
$HO_2^{\bullet} + {}^{\bullet}NO \rightarrow {}^{\bullet}OH + {}^{\bullet}NO_2$	Gas	$8.24 \cdot 10^{-12}$	$cm^3\ s^{-1}$	56,57	16
$HO_2^{\bullet} + {}^{\bullet}NO_2 \rightarrow HO_2NO_2$	Gas	$6.87 \cdot 10^{-13}$	$cm^3\ s^{-1}$	56,57	17
$HO_2NO_2 \rightarrow HO_2^{\bullet} + {}^{\bullet}NO_2$	Gas	$2.49 \cdot 10^{-1}$	s^{-1}	56,57	18
$^{\bullet}OH + HO_2NO_2 \rightarrow NO_2^{\bullet} + H_2O + O_2$	Gas	$2.96 \cdot 10^{-12}$	$cm^3\ s^{-1}$	56,57	19
$HO_2^{\bullet} + {}^{\bullet}NO_3 \rightarrow {}^{\bullet}OH + {}^{\bullet}NO_2$	Gas	$4.00 \cdot 10^{-12}$	$cm^3\ s^{-1}$	56,57	20
$^{\bullet}OH + HONO \rightarrow {}^{\bullet}NO_2 + H_2O$	Gas	$5.78 \cdot 10^{-12}$	$cm^3\ s^{-1}$	56,57	21
$^{\bullet}OH + HNO_3 \rightarrow {}^{\bullet}NO_3 + H_2O$	Gas	$1.37 \cdot 10^{-13}$	$cm^3\ s^{-1}$	56,57	22
$N_2O_5 \rightarrow {}^{\bullet}NO_2 + {}^{\bullet}NO_3$	Gas	$1.83 \cdot 10^{-1}$	s^{-1}	56,57	23
$HO_2NO_2 \rightarrow {}^{\bullet}NO_2 + HO_2^{\bullet}$	Gas	$2.49 \cdot 10^{-1}$	s^{-1}	56,57	24
CI + O_3 → products	Gas	$1.00 \cdot 10^{-13}$	$cm^3\ s^{-1}$	58	25
SPB + $^{\bullet}OH$ → SPB-ox	Surfactant	$1.70 \cdot 10^{-11}$	$cm^3\ s^{-1}$	59–61	26
POG + $^{\bullet}OH$ → POG-ox	Surfactant	$1.70 \cdot 10^{-11}$	$cm^3\ s^{-1}$	26	27
SPB + O_3 → SPB-ox	Surfactant	$1.00 \cdot 10^{-14}$	$cm^3\ s^{-1}$	62,63	28
POG + O_3 → 0.17 H_2O_2	Surfactant	$1.66 \cdot 10^{-16}$	$cm^3\ s^{-1}$	64,65	29
α-Toc + $^{\bullet}OH$ → α-Toc-ox	Surfactant	$4.50 \cdot 10^{-13}$	$cm^3\ s^{-1}$	66	30
α-Toc + O_3 → α-Toc-ox	Surfactant	$1.20 \cdot 10^{-18}$	$cm^3\ s^{-1}$	67	31

$O_2^{\bullet-} + HO_2 \xrightarrow{H_2O} H_2O_2 + OH^- + O_2$	ELF	$1.70 \cdot 10^{-13}$	$cm^3\ s^{-1}$	26,68	32
$HO_2 + HO_2 \rightarrow H_2O_2 + O_2$	ELF	$1.40 \cdot 10^{-15}$	$cm^3\ s^{-1}$	68	33
$O_2^{\bullet-} + O_2^{\bullet-} + 2H^+ \rightarrow H_2O_2 + O_2$	ELF	$3.82 \cdot 10^{-16}$	$cm^3\ s^{-1}$	68	34
$H_2O_2 + {}^{\bullet}OH \rightarrow HO_2 + H_2O$	ELF	$5.50 \cdot 10^{-14}$	$cm^3\ s^{-1}$	69	35
${}^{\bullet}OH + {}^{\bullet}OH \rightarrow H_2O_2$	ELF	$8.60 \cdot 10^{-12}$	$cm^3\ s^{-1}$	70	36
${}^{\bullet}OH + O_2^{\bullet-} \rightarrow O_2 + OH^-$	ELF	$1.30 \cdot 10^{-11}$	$cm^3\ s^{-1}$	59	37
${}^{\bullet}OH + HO_2 \rightarrow H_2O + O_2$	ELF	$1.20 \cdot 10^{-11}$	$cm^3\ s^{-1}$	70	38
$H_2O_2 + HO_2 \rightarrow {}^{\bullet}OH + O_2 + H_2O$	ELF	$4.98 \cdot 10^{-21}$	$cm^3\ s^{-1}$	71	39
$Fe^{2+} + O_2^- + 2H^+ \rightarrow Fe^{3+} + H_2O_2$	ELF	$3.10 \cdot 10^{-14}$	$cm^3\ s^{-1}$	26,68	40
$Fe^{2+} + HO_2 + H^+ \rightarrow Fe^{3+} + H_2O_2$	ELF	$1.99 \cdot 10^{-15}$	$cm^3\ s^{-1}$	72	41
$Fe^{2+} + H_2O_2 \rightarrow Fe^{3+} + {}^{\bullet}OH + OH^-$	ELF	$4.30 \cdot 10^{-18}$	$cm^3\ s^{-1}$	73	42
$Fe^{2+} + {}^{\bullet}OH \rightarrow Fe^{3+} + OH^-$	ELF	$5.30 \cdot 10^{-13}$	$cm^3\ s^{-1}$	74	43
$Fe^{2+} + H_2O_2 \rightarrow Fe^{4+} + H_2O$	ELF	$9.50 \cdot 10^{-18}$	$cm^3\ s^{-1}$	26	44
$Fe^{3+} + H_2O_2 \rightarrow Fe^{2+} + HO_2 + H^+$	ELF	$3.32 \cdot 10^{-24}$	$cm^3\ s^{-1}$	73	45
$Fe^{3+} + HO_2 \rightarrow Fe^{2+} + O_2 + H^+$	ELF	$3.30 \cdot 10^{-18}$	$cm^3\ s^{-1}$	68	46
$Fe^{4+} + Fe^{2+} \rightarrow Fe^{3+} + Fe^{3+}$	ELF	$6.60 \cdot 10^{-18}$	$cm^3\ s^{-1}$	75	47
$Fe^{3+} + Asc \rightarrow Fe^{2+} + Asc^{\bullet}$	ELF	$1.10 \cdot 10^{-19}$	$cm^3\ s^{-1}$	26	48
$Fe^{4+} + Asc \rightarrow Fe^{3+} + Asc^{\bullet}$	ELF	$7.60 \cdot 10^{-19}$	$cm^3\ s^{-1}$	26	49
$Fe^{2+} + O_2 \rightarrow O_2^{\bullet-} + Fe^{3+}$	ELF	$5.20 \cdot 10^{-21}$	$cm^3\ s^{-1}$	26	50
$Cu^+ + HO_2 \xrightarrow{H^+} Cu^{2+} + H_2O_2$	ELF	$2.30 \cdot 10^{-12}$	$cm^3\ s^{-1}$	26	51
$Cu^+ + O_2^{\bullet-} \xrightarrow{H_2O} Cu^{2+} + H_2O_2 + OH^-$	ELF	$5.80 \cdot 10^{-15}$	$cm^3\ s^{-1}$	26	52
$Cu^{2+} + HO_2 \rightarrow Cu^+ + O_2 + H^+$	ELF	$1.60 \cdot 10^{-11}$	$cm^3\ s^{-1}$	26	53
$Cu^{2+} + O_2^{\bullet-} \rightarrow Cu^+ + O_2$	ELF	$8.30 \cdot 10^{-12}$	$cm^3\ s^{-1}$	26	54
$Cu^{2+} + Asc \rightarrow Cu^+ + Asc^{\bullet}$	ELF	$1.40 \cdot 10^{-18}$	$cm^3\ s^{-1}$	26	55
$Cu^+ + O_2 \rightarrow Cu^{2+} + O_2^{\bullet-}$	ELF	$6.90 \cdot 10^{-20}$	$cm^3\ s^{-1}$	26	56
$Cu^+ + H_2O_2 \rightarrow Cu^{2+} + {}^{\bullet}OH + OH^-$	ELF	$2.40 \cdot 10^{-20}$	$cm^3\ s^{-1}$	26	57
$Cu^+ + H_2O_2 \rightarrow Cu^{3+} + OH^- + OH^-$	ELF	$5.00 \cdot 10^{-19}$	$cm^3\ s^{-1}$	26	58
$Cu^+ + Cu^{3+} \rightarrow Cu^{2+} + Cu^{2+}$	ELF	$5.80 \cdot 10^{-12}$	$cm^3\ s^{-1}$	26	59
$Cu^{2+} + H_2O_2 \rightarrow Cu^+ + O_2^{\bullet-} + H^+$	ELF	$3.80 \cdot 10^{-24}$	$cm^3\ s^{-1}$	26	60
$PQN + Asc \rightarrow PQN^{\bullet} + Asc^{\bullet}$	ELF	$1.20 \cdot 10^{-20}$	$cm^3\ s^{-1}$	76	61
$PQN^{\bullet} + O_2 \rightarrow PQN + O_2^{\bullet-}$	ELF	$4.60 \cdot 10^{-13}$	$cm^3\ s^{-1}$	26	62
$PQN^{\bullet} + O_2^{\bullet-} \xrightarrow{2H^+} PQN + H_2O_2$	ELF	$3.30 \cdot 10^{-12}$	$cm^3\ s^{-1}$	26	63
$NQN12 + Asc \rightarrow NQN12^{\bullet} + Asc^{\bullet}$	ELF	$1.50 \cdot 10^{-19}$	$cm^3\ s^{-1}$	76	64
$NQN12^{\bullet} + O_2 \rightarrow NQN12 + O_2^{\bullet-}$	ELF	$4.60 \cdot 10^{-13}$	$cm^3\ s^{-1}$	26	65
$NQN12^{\bullet} + O_2^{\bullet-} \xrightarrow{2H^+} NQN12 + H_2O_2$	ELF	$3.30 \cdot 10^{-12}$	$cm^3\ s^{-1}$	26	66

NQN14 + Asc → NQN14$^{\bullet}$ + Asc$^{\bullet}$	ELF	$6.30 \cdot 10^{-21}$	$cm^3\ s^{-1}$	76	67
NQN14$^{\bullet}$ + O_2 → NQN14 + $O_2^{\bullet-}$	ELF	$4.60 \cdot 10^{-13}$	$cm^3\ s^{-1}$	26	68
NQN14$^{\bullet}$ + $O_2^{\bullet-} \xrightarrow{2H^+}$ NQN14 + H_2O_2	ELF	$3.30 \cdot 10^{-12}$	$cm^3\ s^{-1}$	26	69
UA + O_3 → Products	ELF	$9.60 \cdot 10^{-17}$	$cm^3\ s^{-1}$	67	70
UA + $^{\bullet}OH$ → Products + OH^-	ELF	1.20×10^{-11}	$cm^3\ s^{-1}$	77	71
GSH + $^{\bullet}OH$ → Products + OH^-	ELF	$1.50 \cdot 10^{-11}$	$cm^3\ s^{-1}$	78	72
GSSG + $^{\bullet}OH$ → Products + OH^-	ELF	$1.50 \cdot 10^{-11}$	$cm^3\ s^{-1}$	27	73
Asc$^{\bullet}$ + Asc$^{\bullet} \xrightarrow{H^+}$ Asc + DHA	ELF	$5.00 \cdot 10^{-16}$	$cm^3\ s^{-1}$	79	74
Asc + $O_2^{\bullet-} \xrightarrow{H^+}$ Asc$^{\bullet}$ + H_2O_2	ELF	$5.10 \cdot 10^{-17}$	$cm^3\ s^{-1}$	26	75
Asc + HO_2 → Asc$^{\bullet}$ + H_2O_2	ELF	$2.65 \cdot 10^{-17}$	$cm^3\ s^{-1}$	80	76
Asc + $^{\bullet}OH$ → Products + OH^-	ELF	$1.80 \cdot 10^{-11}$	$cm^3\ s^{-1}$	81	77
Asc + $^{\bullet}O_3$ → Products	ELF	$9.10 \cdot 10^{-17}$	$cm^3\ s^{-1}$	67	78
1.25 GS$^{\bullet}$ + 0.5 O_3 → Products	ELF	$9.60 \cdot 10^{-20}$	$cm^3\ s^{-1}$	67	79
1.25 GSH + 0.5 O_3 → Products	ELF	$9.60 \cdot 10^{-20}$	$cm^3\ s^{-1}$	67	80
GSOO + GSOO → 0.56 $O_2^{\bullet-}$ + Products	ELF	$6.79 \cdot 10^{-13}$	$cm^3\ s^{-1}$	82	81
$O_2^{\bullet-}$ + GSH → GSO$^{\bullet}$ + OH^-	ELF	$3.32 \cdot 10^{-19}$	$cm^3\ s^{-1}$	83–85	82
$NO_2^{\bullet}$ + GS$^{\bullet}$ → $GSNO_2$	ELF	$4.98 \cdot 10^{-12}$	$cm^3\ s^{-1}$	86	83
GSOO$^{\bullet}$ + $NO_2^{\bullet}$ → $GSOONO_2$	ELF	$2.49 \cdot 10^{-12}$	$cm^3\ s^{-1}$	82	84
$GSOONO_2$ → GSOO$^{\bullet}$ + $NO_2^{\bullet}$	ELF	$7.50 \cdot 10^{-1}$	s^{-1}	82	85
$NO_2^{\bullet}$ + GS^- → NO_2^- + GS$^{\bullet}$	ELF	$4.00 \cdot 10^{-13}$	$cm^3\ s^{-1}$	86	86
$NO_2^{\bullet}$ + GSH → NO_2^- + GS$^{\bullet}$ + H^+	ELF	$1.66 \cdot 10^{-14}$	$cm^3\ s^{-1}$	87	87
GSOO$^{\bullet}$ + GSH → GSO$^{\bullet}$ + GSOH	ELF	$3.32 \cdot 10^{-15}$	$cm^3\ s^{-1}$	86	88
GSO + NO_2 → GSOONO	ELF	$7.47 \cdot 10^{-12}$	$cm^3\ s^{-1}$	86	89
GSOONO → Products	ELF	$7.00 \cdot 10^{2}$	s^{-1}	86	90
GS$^{\bullet}$ + GS^- → $GSSG^{\bullet-}$	ELF	$1.59 \cdot 10^{-14}$	$cm^3\ s^{-1}$	86,88	91
$GSSG^{\bullet-}$ → GS$^{\bullet}$ + GS^-	ELF	$1.60 \cdot 10^{5}$	s^{-1}	86,88	92
$GSSG^{\bullet-}$ + O_2 → GSSG + $O_2^{\bullet-}$	ELF	$8.30 \cdot 10^{-12}$	$cm^3\ s^{-1}$	86,88	93
GS$^{\bullet}$ + GS$^{\bullet}$ → GSSG	ELF	$8.30 \cdot 10^{-12}$	$cm^3\ s^{-1}$	88	94
GSOH + GSH → GSSG + H_2O	ELF	$1.20 \cdot 10^{-18}$	$cm^3\ s^{-1}$	89	95
GSO$^{\bullet}$ + GSO$^{\bullet}$ → Products	ELF	$9.96 \cdot 10^{-14}$	$cm^3\ s^{-1}$	86	96
GS^- + H_2O_2 → GSOH + OH^-	ELF	$1.60 \cdot 10^{-21}$	$cm^3\ s^{-1}$	89	97
GS$^{\bullet}$ + Asc → GSH + Asc$^{\bullet}$	ELF	$1.00 \cdot 10^{-12}$	$cm^3\ s^{-1}$	90,91	98
UA + $NO_2^{\bullet}$ → UA$^{\bullet}$ + NO_2^-	ELF	$3.00 \cdot 10^{-14}$	$cm^3\ s^{-1}$	92,93	99
Asc + $NO_2^{\bullet}$ → Asc$^{\bullet}$ + NO_2^-	ELF	$5.80 \cdot 10^{-14}$	$cm^3\ s^{-1}$	92,93	100
UA$^{\bullet}$ + Asc → UA + Asc$^{\bullet}$	ELF	$1.70 \cdot 10^{-15}$	$cm^3\ s^{-1}$	91	101

$GS^{\bullet} + UA \rightarrow GSH + UA^{\bullet}$	ELF	$5.00 \cdot 10^{-14}$	$cm^3\ s^{-1}$	87	102
$O_2^{\bullet-} + NO_2^{\bullet} \rightarrow O_2NOO^-$	ELF	$7.50 \cdot 10^{-12}$	$cm^3\ s^{-1}$	86,94	103
$O_2NOO^- \rightarrow NO_2^- + O_2$	ELF	$7.00 \cdot 10^{-1}$	s^{-1}	86	104
$O_2NOO^- \rightarrow O_2^{\bullet-} + NO_2^{\bullet}$	ELF	1.10	s^{-1}	86	105
$NO_2^{\bullet} + NO_2^{\bullet} \rightarrow N_2O_4$	ELF	$7.50 \cdot 10^{-13}$	$cm^3\ s^{-1}$	27	106
$N_2O_4 \rightarrow NO_2^{\bullet} + NO_2^{\bullet}$	ELF	$6.90 \cdot 10^{3}$	s^{-1}	27	107
$N_2O_4 \xrightarrow{H_2O} NO_2^- + NO_3^- + 2H^+$	ELF	$1.00 \cdot 10^{3}$	s^{-1}	86	108
$O_2^{\bullet-} + O_3 \xrightarrow{H_2O} {}^{\bullet}OH + 2O_2 + OH^-$	ELF	$2.50 \cdot 10^{-12}$	$cm^3\ s^{-1}$	95	109
$HO_2 + O_3 \rightarrow {}^{\bullet}OH + 2O_2$	ELF	$1.66 \cdot 10^{-17}$	$cm^3\ s^{-1}$	95	110
$NO_2^- + {}^{\bullet}OH \rightarrow NO_2^{\bullet} + OH^-$	ELF	$8.80 \cdot 10^{-12}$	$cm^3\ s^{-1}$	94	111
${}^{\bullet}OH + NO_2^{\bullet} \rightarrow NO_3^- + H^+$	ELF	$7.50 \cdot 10^{-12}$	$cm^3\ s^{-1}$	86	112
${}^{\bullet}OH + NO_2^{\bullet} \rightarrow ONOOH$	ELF	$7.50 \cdot 10^{-12}$	$cm^3\ s^{-1}$	86	113
$ONOOH \rightarrow NO_2^{\bullet} + {}^{\bullet}OH$	ELF	$3.00 \cdot 10^{-1}$	s^{-1}	86	114
$ONOOH \rightarrow NO_3^- + H^+$	ELF	$7.00 \cdot 10^{-1}$	s^{-1}	86	115
$ONOO^- + GSH \rightarrow NO_2^- + GSOH$	ELF	$1.10 \cdot 10^{-18}$	$cm^3\ s^{-1}$	96	116
$GSO^{\bullet} + NO_2^{\bullet} \rightarrow GSOONO$	ELF	$7.50 \cdot 10^{-12}$	$cm^3\ s^{-1}$	86	117
$GSOONO \xrightarrow{H_2O} Products$	ELF	$7.00 \cdot 10^{2}$	s^{-1}	86	118
$ONOOH + Asc \rightarrow Im_1$	ELF	$1.66 \cdot 10^{-15}$	$cm^3\ s^{-1}$	97	119
$Im_1 \rightarrow ONOOH + Asc$	ELF	$5.00 \cdot 10^{2}$	s^{-1}	97	120
$Im_1 \rightarrow Im_2$	ELF	$4.00 \cdot 10^{1}$	s^{-1}	97	121
$Im_2 \rightarrow Im_1$	ELF	5.00	s^{-1}	97	122
$Im_2 + Asc \rightarrow Asc + DHA + NO_2^- + H_2O$	ELF	$1.66 \cdot 10^{-19}$	$cm^3\ s^{-1}$	97	123
$Im_2 \rightarrow Asc + NO_3^- + H^+$	ELF	$8.50 \cdot 10^{-1}$	$cm^3\ s^{-1}$	97	124
$ONOOH + UA \rightarrow UA^{rad} + NO_2 +$ Products	ELF	$2.60 \cdot 10^{-19}$	$cm^3\ s^{-1}$	97	125
$O_2^{\bullet-} + SOD \xrightarrow{H^+} 0.5\ H_2O_2 + SOD$	ELF	$2.65 \cdot 10^{-12}$	$cm^3\ s^{-1}$	27	126
$H_2O_2 +$ catalase $\rightarrow H_2O + 0.5\ O_2 +$ catalase	ELF	$3.20 \cdot 10^{-14}$	$cm^3\ s^{-1}$	27	127
${}^{\bullet}OH +$ organic matter $\rightarrow$ oxidized organic matter	ELF	$1.66 \cdot 10^{-12}$	$cm^3\ s^{-1}$	77,98	128
$\rightarrow H_2O_2$	Cells	$1 \cdot 10^{14}$	$cm^{-3}\ s^{-1}$	this study	129
$H_2O_2 +$ enzymes $\rightarrow H_2O + O_2 +$ enzymes	Cells	$3.32 \cdot 10^{-14}$	$cm^3\ s^{-1}$	27	130
$O_2^{\bullet-} + SOD \xrightarrow{H^+} 0.5\ H_2O_2 + SOD$	Cells	$2.65 \cdot 10^{-12}$	$cm^3\ s^{-1}$	27	131

Table S2. Concentrations of gas-phase pollutants considered in the examined pollution scenarios (Fig. 3). The NO_2 levels represent a 1:1 mass ratio with PM2.5 levels[27].

	Remote	**Rural**	**Indoor**	**Heavily cleaned indoor**	**Clean urban**	**Polluted urban**
O_3 (ppb)	15 [99]	20 [2]	10 [100]	10 [100]	30 [2]	75 [101]
H_2O_2 (ppb)	0.2 [102]	0.5 [4]	0.9 [103,104]	280 [105]	1 [3]	2 [5]
NO_2 (ppb)	2.1	4.2	5.3	5.3	15.9	31.9
PM2.5 ($\mu g \cdot m^{-3}$)	4 [106]	8 [107,108]	10 [109]	10 [109]	30 [2]	60 [110,111]

Table S3. Overview of important and default input parameters for KM-SUB-ELF 2.0 in the standard pollution scenario.

Parameter	**Value**	**Unit**
PM2.5 concentration	30	$\mu g\ m^{-3}$
NO_2 concentration	30	$\mu g\ m^{-3}$
O_3 concentration	30	ppb
Concentration of ambient H_2O_2	1	ppb
Concentration of blood H_2O_2	5	µM
Effective membrane permeability of H_2O_2	1×10^{-5}	$cm\ s^{-1}$
H_2O_2 production in the cell layer	1×10^{14}	$cm^{-3}\ s^{-1}$
Concentration of H_2O_2-scavenging enzymes in cells	10	µM

Table S4. Input parameters of the model KM-SUB-ELF 2.0.

Parameter	Value	Unit
Henry's law equilibrium constant of O_3	$1.0 \cdot 10^{-2}$	M atm^{-1}
Henry's law equilibrium constant of H_2O_2	$9.1 \cdot 10^{4}$	M atm^{-1}
Henry's law equilibrium constant of $^{\bullet}OH$	29	M atm^{-1}
Henry's law equilibrium constant of $HO_2^{\bullet}$	$6.8 \cdot 10^{2}$	M atm^{-1}
Particulate mass fraction of Cu^{2+}	$3.1 \cdot 10^{-4}$	-
Particulate mass fraction of Fe^{2+}	$8.1 \cdot 10^{-3}$	-
Particulate mass fraction of quinones	$1.9 \cdot 10^{-5}$	-
Particulate mass fraction of SOA	0.33	-
Water soluble fraction of Cu^{2+}	0.40	-
Water soluble fraction of Fe^{2+}	0.10	-
Water soluble fraction of quinones	0.10	-
Water soluble fraction of SOA	0.10	-
Particulate exposure time	2	h
ELF catalase concentration	5	pM
ELF superoxide dismutase concentration	1000	pM
ELF glutathione concentration	108	μM
ELF ascorbate concentration	40	μM
ELF uric acid concentration	200	μM
ELF α-Tocopherol concentration	0.7	μM
ELF SP-$B_{1\text{-}25}$ concentration	5000	μM
ELF POG concentration	13000	μM
ELF organic matter concentration	40000	μM
PM2.5 accumulation time	2	h
PM2.5 deposition factor	0.45	-
Functional residual capacity of respiratory tract	2750	cm^3
Tidal volume	1500	cm^3
Duration of breath	3.67	sec
ELF pH	7	-
ELF volume	20	cm^3
Respiratory tract surface area	$8.9 \cdot 10^{5}$	cm^2
Respiratory tract temperature	310	K
Cellular concentration of H_2O_2-scavenging enzymes	10	μM
H_2O_2 effective membrane permeability coefficient	$1 \cdot 10^{-5}$ $(4 \cdot 10^{-6} - 40 \cdot 10^{-5})$	cm s^{-1}
H_2O_2 production in the cell layer	$1 \cdot 10^{14}$	cm^{-3} s^{-1}
Thickness of cell membrane	$1 \cdot 10^{-4}$	cm
Ambient H_2O_2 concentration	1	ppb
Blood H_2O_2 concentration	5	μM

Table S5. Literature values for H_2O_2 ambient and indoor concentrations.

Concentration (ppb)	Region	Reference
1.0	Indoor	Li et al., 2002 [103]
0.1-1.5	Workplace	Christensen et al., 2000 [112]
0.1-5	California	Kok et al., 1978 [3]
0.5	North Carolina	Das & Anjela, 1994 [4]
2.0	Beijing	He et al., 2010 [5]
≤1.5	Nagoya	Watanabe & Tanaka, 1995 [6]
0.5-4.5	Remote Beijing	Weihan et al., 1998 [7]

References

1 D. Vione, V. Maurino, C. Minero and E. Pelizzetti, The atmospheric chemistry of hydrogen peroxide: A review, *Ann. Chim.*, 2003, **93**, 477–488.

2 J. H. Seinfeld, S. N. Pandis, *Atmospheric Chemistry and Physics: From Air Pollution to Climate Change*, 3rd Edition, 2016.

3 G. L. Kok, K. R. Darnall, A. M. Winer, J. N. Pitts and B. W. Gay, Ambient Air Measurements of Hydrogen Peroxide in the California South Coast Air Basin, *Environ. Sci. Technol.*, 1978, **12**, 1077–1080.

4 V. P. Aneja, Analysis of gaseous hydrogen peroxide concentrations in raleigh, north carolina, *Air Waste*, 1994, **44**, 176–183.

5 S. Z. He, Z. M. Chen, X. Zhang, Y. Zhao, D. M. Huang, J. N. Zhao, T. Zhu, M. Hu and L. M. Zeng, Measurement of atmospheric hydrogen peroxide and organic peroxides in Beijing before and during the 2008 Olympic Games: Chemical and physical factors influencing their concentrations, *J. Geophys. Res*, 2010, **115**, 1-12.

6 K. Watanabe, H. Tanaka Measurement of gaseous hydrogen peroxide (H2O2) concentrations in the urban atmosphere. *J. Meteo. Soc. Japan.*, 1995, **73**, 839-847.

7 S. Weihan, L. Wei, D. Guoan and W. E. Wilson, A study on hydrogen peroxide in the atmosphere, *Adv. Atmos. Sci.*, 1989, **6**, 509–515.

8 D. Ezeriņa, B. Morgan and T. P. Dick, Imaging dynamic redox processes with genetically encoded probes, *J. Mol. Cell. Cardiol.*, 2014, **73**, 43–49.

9 O. Lyublinskaya and F. Antunes, Measuring intracellular concentration of hydrogen peroxide with the use of genetically encoded H 2 O 2 biosensor HyPer, *Redox Biol.*, 2019, **24**, 101200.

10 M. B. Schleiss, O. Holz, M. Behnke, K. Richter, H. Magnussen and R. A. Jörres, The concentration of hydrogen peroxide in exhaled air depends on expiratory flow rate, *Eur. Respir. J.*, 2000, **16**, 1115–1118.

11 J. R. Stone, S. Yang, Hydrogen Peroxide: A Signaling Messenger. *Antiox. Red. Sign.*, 2006, **8**, 243-271.

12 H. Sies, Hydrogen peroxide as a central redox signaling molecule in physiological oxidative stress: Oxidative eustress, *Redox Biol.*, 2017, **11**, 613–619.

13 W. J. C. Van Beurden, G. A. Harff, P. N. R. Dekhuijzen, M. J. A. Van Den Bosch, J. P. H. M. Creemers and F. W. J. M. Smeenk, An efficient and reproducible method for measuring hydrogen peroxide in exhaled breath condensate, *Respir. Med.*, 2002, **96**, 197–203.

14 C. Caffarelli, E. Calcinai, L. Rinaldi, C. Povesi Dascola, L. Terracciano and M. Corradi, Hydrogen peroxide in exhaled breath condensate in asthmatic children during acute exacerbation and after treatment, *Respiration*, 2012, **84**, 291–298.

15 W. B. Gerritsen, P. Zanen, A. A. Bauwens, J. M. van den Bosch and F. J. Haas, Validation of a new method to measure hydrogen peroxide in exhaled breath condensate, *Respir. Med.*, 2005, **99**, 1132–1137.

16 H. Knobloch, G. Becher, M. Decker and P. Reinhold, Evaluation of H2O2 and pH in exhaled breath condensate samples: Methodical and physiological aspects, *Biomarkers*, 2008, **13**, 319–341.

17 C. Nagaraja, B. L. Shashibhushan, Sagar, M. Asif and P. H. Manjunath, Hydrogen peroxide in exhaled breath condensate: A clinical study, *Lung India*, 2012, **29**, 123–127.

18 M. E. Quimbar, S. Q. Davis, S. T. Al-Farra, A. Hayes, V. Jovic, M. Masuda and A. R. Lippert, Chemiluminescent Measurement of Hydrogen Peroxide in the Exhaled Breath Condensate of Healthy and Asthmatic Adults, *Anal. Chem.*, 2020, **92**, 14594–14600.

19 M. R. Branco, H. S. Marinho, L. Cyrne and F. Antunes, Decrease of H 2O 2 Plasma Membrane Permeability during Adaptation to H 2O 2 in Saccharomyces cerevisiae, *J. Biol. Chem.*, 2004, **279**, 6501–6506.

20 F. Antunes and P. M. Brito, Quantitative biology of hydrogen peroxide signaling, *Redox Biol.*, 2017, **13**, 1–7.

21 R. Gaikwad, P. R. Thangaraj and A. K. Sen, Direct and rapid measurement of hydrogen peroxide in human blood using a microfluidic device, *Sci. Rep.*, 2021, **11**, 1–10.

22 R. Bretón-Romero and S. Lamas, Hydrogen peroxide signaling in vascular endothelial cells, *Redox Biol.*, 2014, **2**, 529–534.

23 E. Dicker and A. I. Cederbaum, Increased NADH-dependent production of reactive oxygen intermediates by microsomes after chronic ethanol consumption: Comparisons with NADPH, *Arch. Biochem. Biophys.*, 1992, **293**, 274–280.

24 H. J. Forman, A. Bernardo and K. J. A. Davies, What is the concentration of hydrogen

peroxide in blood and plasma?, *Arch. Biochem. Biophys.*, 2016, **603**, 48–53.

25 B. Halliwell, M. V. Clement, J. Ramalingam and Lee Hua Long, Hydrogen peroxide. Ubiquitous in cell culture and in vivo?, *IUBMB Life*, 2000, **50**, 251–257.

26 P. S. J. Lakey, T. Berkemeier, H. Tong, A. M. Arangio, K. Lucas, U. Pöschl and M. Shiraiwa, Chemical exposure-response relationship between air pollutants and reactive oxygen species in the human respiratory tract, *Sci. Rep.*, 2016, **6**, 1–6.

27 S. Lelieveld, J. Wilson, E. Dovrou, A. Mishra, P. S. J. Lakey, M. Shiraiwa, U. Pöschl and T. Berkemeier, Hydroxyl Radical Production by Air Pollutants in Epithelial Lining Fluid Governed by Interconversion and Scavenging of Reactive Oxygen Species, *Environ. Sci. Technol.*, 2021, **55**. 14069-14079.

28 I. S. Mudway and F. J. Kelly, Ozone and the lung: A sensitive issue, *Mol. Aspects Med.*, 2000, **21**, 1–48.

29 A. Van Der Vliet, C. A. O'Neill, C. E. Cross, J. M. Koostra, W. G. Volz, B. Halliwell and S. Louie, Determination of low-molecular-mass antioxidant concentrations in human respiratory tract lining fluids, *Am. J. Physiol. - Lung Cell. Mol. Physiol.*, 1999, **276**, 289–296.

30 A. M. Cantin, G. A. Fells, R. C. Hubbard and R. G. Crystal, Antioxidant macromolecules in the epithelial lining fluid of the normal human lower respiratory tract, *J. Clin. Invest.*, 1990, **86**, 962–971.

31 H. Aebi, [13] Catalase in Vitro, *Methods Enzymol.*, 1984, **105**, 121–126.

32 B. P. Jones and A. Suggett, The Catalase-Hydrogen Peroxide System, *Biochem. J.*, 1968, **110**, 621–629.

33 J. A. Fee and C. Bull, Steady-state kinetic studies of superoxide dismutases. Saturative behavior of the copper- and zinc-containing protein, *J. Biol. Chem.*, 1986, **261**, 13000–13004.

34 A. Bar-Even, E. Noor, Y. Savir, W. Liebermeister, D. Davidi, D. S. Tawfik and R. Milo, The moderately efficient enzyme: Evolutionary and physicochemical trends shaping enzyme parameters, *Biochemistry*, 2011, **50**, 4402–4410.

35 G. B. Smejkal and S. Kakumanu, Enzymes and their turnover numbers, *Expert Rev. Proteomics*, 2019, **16**, 543–544.

36 S. P. Andreoli, C. Mallett, J. A. McAteer and L. V. Williams, Antioxidant defense mechanisms of endothelial cells and renal tubular epithelial cells In Vitro: Role of the glutathione redox cycle and catalase, *Pediatr. Res.*, 1992, **32**, 360–365.

37 C. N. Scaglione, Q. Xu, V. K. Ramanujan, Direct measurement of catalase activity in living cells and tissue biopsies. *Biochem. Biophys. Res. Commun.*. **470**, 191-196 (2017).

38 C. C. Winterbourn and M. B. Hampton, Thiol chemistry and specificity in redox signaling, *Free Radic. Biol. Med.*, 2008, **45**, 549–561.

39 A. Tovar-Méndez, M. A. Matamoros, P. Bustos-Sanmamed, K. J. Dietz, F. J. Cejudo, N. Rouhier, S. Sato, S. Tabata and M. Becana, Peroxiredoxins and NADPH-dependent thioredoxin systems in the model legume lotus japonicus, *Plant Physiol.*, 2011, **156**, 1535–1547.

40 V. Castranova, J. Rabovsky, J. H. Tucker and P. R. Miles, The alveolar type II epithelial cell: A multifunctional pneumocyte, *Toxicol. Appl. Pharmacol.*, 1988, **93**, 472–483.

41 V. L. Kinnula, J. I. Everitt, A. R. Whorton and J. D. Crapo, Hydrogen peroxide production by alveolar type II cells, alveolar macrophages, and endothelial cells, *Am. J. Physiol. - Lung Cell. Mol. Physiol.*, 1991, **261**, L84-L91.

42 W. J. Piotrowski, J. Marczak, D. Dinsdale, Z. Kurmanowska, Y. Tarasow, J. Komos and D. Nowak, Release of hydrogen peroxide by rat type II pneumocytes in the prolonged culture, *Toxicol. Vitr.*, 2000, **14**, 85–93.

43 K. R. Albe, M. H. Butler and B. E. Wright, Cellular concentrations of enzymes and their substrates, *J. Theor. Biol.*, 1990, **143**, 163–195.

44 J. L. Jimenez, M. R. Canagaratna, N. M. Donahue, A. S. H. Prevot, Q. Zhang, J. H. Kroll, P. F. DeCarlo, J. D. Allan, H. Coe, N. L. Ng, A. C. Aiken, K. S. Docherty, I. M. Ulbrich, A. P. Grieshop, A. L. Robinson, J. Duplissy, J. D. Smith, K. R. Wilson, V. A. Lanz, C. Hueglin, Y. L. Sun, J. Tian, A. Laaksonen, T. Raatikainen, J. Rautiainen, P. Vaattovaara, M. Ehn, M. Kulmala, J. M. Tomlinson, D. R. Collins, M. J. Cubison, E. J. Dunlea, J. A. Huffman, T. B. Onasch, M. R. Alfarra, P. I. Williams, K. Bower, Y. Kondo, J. Schneider, F. Drewnick, S. Borrmann, S. Weimer, K. Demerjian, D. Salcedo, L. Cottrell, R. Griffin, A. Takami, T. Miyoshi, S. Hatakeyama, A. Shimono, J. Y. Sun, Y. M. Zhang, K. Dzepina, J. R. Kimmel, D. Sueper, J. T. Jayne, S. C. Herndon, A. M. Trimborn, L. R. Williams, E. C. Wood, A. M. Middlebrook, C. E. Kolb, U. Baltensperger and D. R. Worsnop, Evolution of organic aerosols in the atmosphere, *Science*, 2009, **326**, 1525–1529.

45 M. Hallquist, J. C. Wenger, U. Baltensperger, Y. Rudich, D. Simpson, M. Claeys, J. Dommen, N. M. Donahue, C. George, A. H. Goldstein, J. F. Hamilton, H. Herrmann, T. Hoffmann, Y. Iinuma, M. Jang, M. E. Jenkin, J. L. Jimenez, A. Kiendler-Scharr, W. Maenhaut, G. McFiggans, T. F. Mentel, A. Monod, A. S. H. Prévôt, J. H. Seinfeld, J. D. Surratt, R. Szmigielski and J. Wildt, The formation, properties and impact of secondary organic aerosol: Current and emerging issues, *Atmos. Chem. Phys.*, 2009, **9**, 5155–5236.

46 K. S. Docherty, W. Wu, Y. Bin Lim and P. J. Ziemann, Contributions of organic peroxides to secondary aerosol formed from reactions of monoterpenes with O 3, *Environ. Sci. Technol.*, 2005, **39**, 4049–4059.

47 M. Krapf, I. El Haddad, E. A. Bruns, U. Molteni, K. R. Daellenbach, A. S. H. Prévôt, U. Baltensperger and J. Dommen, Labile Peroxides in Secondary Organic Aerosol, *Chem*, 2016, **1**, 603–616.

48 H. Tong, A. M. Arangio, P. S. J. Lakey, T. Berkemeier, F. Liu, C. J. Kampf, W. H. Brune, U. Poschl and M. Shiraiwa, Hydroxyl radicals from secondary organic aerosol decomposition in water, *Atmos. Chem. Phys.*, 2016, **16**, 1761–1771.

49 Y. Wang, H. Kim and S. E. Paulson, Hydrogen peroxide generation from α- and β-pinene and toluene secondary organic aerosols, *Atmos. Environ.*, 2011, **45**, 3149–3156.

50 P. H. Chowdhury, Q. He, R. Carmieli, C. Li, Y. Rudich and M. Pardo, Connecting the Oxidative Potential of Secondary Organic Aerosols with Reactive Oxygen Species in Exposed Lung Cells, *Environ. Sci. Technol.*, 2019, **53**, 13949–13958.

51 J. Wei, T. Fang, P. S. J. Lakey and M. Shiraiwa, Iron-Facilitated Organic Radical Formation from Secondary Organic Aerosols in Surrogate Lung Fluid, *Environ. Sci. Technol.*, 2022, **56(11)**, 7234-7243.

52 Z. H. Zhang, E. Hartner, B. Utinger, B. Gfeller, A. Paul, M. Sklorz, H. Czech, B. X. Yang, X. Y. Su, G. Jakobi, J. Orasche, J. Schnelle-Kreis, S. Jeong, T. Gröger, M. Pardo, T. Hohaus, T. Adam, A. Kiendler-Scharr, Y. Rudich, R. Zimmermann and M. Kalberer, Are reactive oxygen species (ROS) a suitable metric to predict toxicity of carbonaceous aerosol particles?, *Atmos. Chem. Phys.*, 2022, **22**, 1793–1809.

53 J. Wei, T. Fang, C. Wong, P. S. J. Lakey, S. A. Nizkorodov and M. Shiraiwa, Superoxide Formation from Aqueous Reactions of Biogenic Secondary Organic Aerosols, *Environ. Sci. Technol.*, 2021, **55**, 260–270.

54 H. Tong, P. S. J. Lakey, A. M. Arangio, J. Socorro, F. Shen, K. Lucas, W. H. Brune, U. Pöschl and M. Shiraiwa, Reactive Oxygen Species Formed by Secondary Organic Aerosols in Water and Surrogate Lung Fluid, *Environ. Sci. Technol.*, 2018, **52**, 11642–11651.

55 T. Fang, Y. Huang, J. Wei, J. E. M. Mena, P. S. J. Lakey, M. T. Kleinman, M. A. Digman and M. Shiraiwa, Superoxide Release by Macrophages through NADPH Oxidase Activation Dominating Chemistry by Isoprene Secondary Organic Aerosols and Quinones to Cause Oxidative Damage on Membranes, 2022, **56(23)**, 17029-17038.

56 S. M. Saunders, M. E. Jenkin, R. G. Derwent and M. J. Pilling, Protocol for the development of the Master Chemical Mechanism, MCM v3 (Part A): Tropospheric degradation of non-aromatic volatile organic compounds, *Atmos. Chem. Phys.*, 2003, **3**, 161–180.

57 M. E. Jenkin, S. M. Saunders, V. Wagner and M. J. Pilling, Protocol for the development of the Master Chemical Mechanism, MCM v3 (Part B): Tropospheric degradation of aromatic volatile organic compounds, *Atmos. Chem. Phys.*, 2003, **3**, 181–193.

58 Y. P. Chang, H. H. Chang and J. J. M. Lin, Kinetics of the simplest Criegee intermediate reaction with ozone studied using a mid-infrared quantum cascade laser spectrometer, *Phys. Chem. Chem. Phys.*, 2017, **20**, 97–102.

59 G. V. Buxton, C. L. Greenstock, W. P. Helman and A. B. Ross, Critical Review of rate constants for reactions of hydrated electrons, hydrogen atoms and hydroxyl radicals (·OH/·O− in Aqueous Solution, *J. Phys. Chem. Ref. Data*, 1988, **17**, 513–886.

60 M. Simic, P. Neta and E. Hayon, Pulse radiolysis study of alcohols in aqueous solution, *J. Phys. Chem.*, 1969, **73**, 3794–3800.

61 M. J. Zhao, L. Jung, C. Tanielian and R. Mechin, Kinetics of the competitive degradation of deoxyribose and other biomolecules by hydroxyl radicals produced by the fenton reaction, *Free Radic. Res.*, 1994, **20**, 345–363.

62 Kanofsky, J. R. & Sima, P. D. Reactive absorption of ozone by aqueous biomolecule solutions: Implications for the role of sulfhydryl compounds as targets for ozone. *Arch Biochem Biophys.,* 1995, **316**, 52-62.

63 W. A. Pryor, D. H. Giamalva and D. F. Church, Kinetics of Ozonation. 2. Amino Acids and Model Compounds in Water and Comparisons to Rates in Nonpolar Solvents, *J. Am. Chem. Soc.*, 1984, **106**, 7094–7100.

64 P. Neeb, F. Sauer, O. Horie and G. K. Moortgat, Formation of hydroxymethyl hydroperoxide and formic acid in alkene ozonolysis in the presence of water vapour, *Atmos. Environ.*, 1997, **31**, 1417–1423.

65 M. Zeng, N. Heine and K. R. Wilson, Evidence that criegee intermediates drive autoxidation in unsaturated lipids, *Proc. Natl. Acad. Sci. U. S. A.*, 2020, **117**, 4486–4490.

66 M. Navarrete, C. Rangel, J. C. Corchado and J. Espinosa-García, Trapping of the OH radical by α-tocopherol: A theoretical study, *J. Phys. Chem. A*, 2005, **109**, 4777–4784.

67 S. Kermani, A. Ben-Jebria and J. S. Ultman, Kinetics of ozone reaction with uric acid, ascorbic acid, and glutathione at physiologically relevant conditions, *Arch. Biochem. Biophys.*, 2006, **451**, 8–16.

68 J. D. Rush and B. H. J. Bielski, Pulse radiolytic studies of the reactions of HO2/O2- with Fe(II)/Fe(III) ions. The reactivity of HO2/O2- with ferric ions and its implication on the occurrence of the Haber-Weiss reaction, *J. Phys. Chem.*, 1985, **89**, 5062–5066.

69 H. Christensen, K. Sehested and H. Corfitzen, Reactions of hydroxyl radicals with hydrogen peroxide at ambient and elevated temperatures, *J. Phys. Chem.*, 1982, **86**, 1588–1590.

70 K. Sehested, O. L. Rasmussen and H. Fricke, Rate constants of OH with HO2, O2-, and H2O2+ from hydrogen peroxide formation in pulse-irradiated oxygenated water, *J. Phys. Chem.*, 1968, **72**, 626–631.

71 W. H. Koppenol, The Haber-Weiss cycle - 70 years later, *Redox Rep.*, 2001, **6**, 229–234.

72 G. G. Jayson, B. J. Parsons and A. J. Swallow, Oxidation of ferrous ions by hydroxyl

radicals, *J. Chem. Soc. Faraday Trans. 1 Phys. Chem. Condens. Phases*, 1972, **68**, 2053–2058.

73 S. Lewis, A. Lynch, L. Bachas, S. Hampson, L. Ormsbee and D. Bhattacharyya, Chelate-modified fenton reaction for the degradation of trichloroethylene in aqueous and two-phase systems, *Environ. Eng. Sci.*, 2009, **26**, 849–859.

74 Z. Stuglik and Z. PawełZagórski, Pulse radiolysis of neutral iron(II) solutions: oxidation of ferrous ions by OH radicals, *Radiat. Phys. Chem.*, 1981, **17**, 229–233.

75 S. J. Hug and O. Leupin, Iron-catalyzed oxidation of Arsenic(III) by oxygen and by hydrogen peroxide: pH-dependent formation of oxidants in the Fenton reaction, *Environ. Sci. Technol.*, 2003, **37**, 2734–2742.

76 J. G. Charrier, A. S. McFall, N. K. Richards-Henderson and C. Anastasio, Hydrogen peroxide formation in a surrogate lung fluid by transition metals and quinones present in particulate matter, *Environ. Sci. Technol.*, 2014, **48**, 7010–7017.

77 Masuda, T., Shinohara, H. & Kondo, M. Reactions of hydroxyl radicals with nucleic acid bases and the related compounds in gamma-irradiated aqueous solution. *J. Radiat. Res.*, 1975, **16**, 153-161.

78 M. Liphard, E. Bothe and D. Schulte-Frohlinde, The influence of glutathione on single-Strand breakage in single-stranded DNA irradiated in aqueous solution in the absence and presence of oxygen, *Int. J. Radiat. Biol.*, 1990, **58**, 589–602.

79 W. V. Drigalski, Vitamin C in urine in health and disease., *Klin. Wochenschr.*, 1935, **14**, 338–339.

80 J. Shen, P. T. Griffiths, S. J. Campbell, B. Utinger, M. Kalberer and S. E. Paulson, Ascorbate oxidation by iron, copper and reactive oxygen species: review, model development, and derivation of key rate constants, *Sci. Rep.*, 2021, **11**, 1–14.

81 B. D. Adams, G.E., Boag, J.W., Currant, J. and Michael, Absolute rate constants for the reaction of the hydroxyl radical with organic compounds, *Pulse radiolysis*, 1965, 131–143.

82 S. Goldstein, J. Lind and G. Merenyi, Reaction of Organic Peroxyl Radicals with ṄO2 and ṄO in Aqueous Solution: Intermediacy of Organic Peroxynitrate and Peroxynitrite Species, *J. Phys. Chem. A*, 2004, **108**, 1719–1725.

83 C. M. Jones, A. Lawrence, P. Wardman and M. J. Burkitt, Electron paramagnetic resonance spin trapping investigation into the kinetics of glutathione oxidation by the superoxide radical: Re-evaluation of the rate constant, *Free Radic. Biol. Med.*, 2002, **32**, 982–990.

84 C. C. Winterbourn, Revisiting the reactions of superoxide with glutathione and other thiols, *Arch. Biochem. Biophys.*, 2016, **595**, 68–71.

85 H. Wefers and H. Sies, Oxidation of glutathione by the superoxide radical to the disulfide and the sulfonate yielding singlet oxygen, *Eur. J. Biochem.*, 1983, **137**, 29–36.

86 M. Kirsch, M. Lehnig, H. G. Korth, R. Sustmann and H. De Groot, Inhibition of peroxynitrite-induced nitration of tyrosine by glutathione in the presence of carbon dioxide through both radical repair and peroxynitrate formation, *Chem. - A Eur. J.*, 2001, **7**, 3313–3320.

87 E. Ford, M. N. Hughes and P. Wardman, Kinetics of the reactions of nitrogen dioxide with glutathione, cysteine, and uric acid at physiological pH, *Free Radic. Biol. Med.*, 2002, **32**, 1314–1323.

88 P. Wardman and C. von Sonntag, Kinetic factors that control the fate of thiyl radicals in cells, *Methods Enzymol.*, 1995, **251**, 31–45.

89 D. Luo, S. W. Smith and B. D. Anderson, Kinetics and mechanism of the reaction of cysteine and hydrogen peroxide in aqueous solution, *J. Pharm. Sci.*, 2005, **94**, 304–316.

90 B. S. Winkler, S. M. Orselli and T. S. Rex, The redox couple between glutathione and ascorbic acid: A chemical and physiological perspective, *Free Radic. Biol. Med.*, 1994, **17**, 333–349.

91 G. R. Buettner, B. A. Jurkiewicz, N. May, G. R. Buettner and B. A. Jurkiewicz, Catalytic Metals , Ascorbate and Free Radicals : Combinations to Avoid Linked references are available on JSTOR for this article : Catalytic Metals , Ascorbate and Free Radicals : Combinations to Avoid ', 2018, **145**, 532–541.

92 Z. B. Alfassi, R. E., Huie, P. Neta, P., L. C. T. Shoute, Temperature dependence of the rate constats for reaction of inorganic radicals with organic reductants. *J. Phys. Chem.*, 1990, **94**, 8800–8805.

93 O. Augusto, M. G. Bonini, A. M. Amanso, E. Linares, C. C. X. Santos and S. L. De Menezes, Nitrogen dioxide and carbonate radical anion: Two emerging radicals in biology, *Free Radic. Biol. Med.*, 2002, **32**, 841–859.

94 S. Goldstein and G. Czapski, Reactivity of peroxynitrite versus simultaneous generation of ·NO and O2·- toward NADH, *Chem. Res. Toxicol.*, 2000, **13**, 736–741.

95 D. J. Jacob, Heterogeneous chemistry and tropospheric ozone, *Atmos. Environ.*, 2000, **34**, 2131–2159.

96 M. G. Bonini and O. Augusto, Carbon Dioxide Stimulates the Production of Thiyl, Sulfinyl, and Disulfide Radical Anion from Thiol Oxidation by Peroxynitrite, *J. Biol. Chem.*, 2001, **276**, 9749–9754.

97 C. R. Kurz, R. Kissner, T. Nauser, D. Perrin and W. H. Koppenol, Rapid scavenging of peroxynitrous acid by monohydroascorbate, *Free Radic. Biol. Med.*, 2003, **35**, 1529–1537.

98 W. A. Pryor Oxy-radicals and related and reactions: Their formation, lifetimes, and reactions. *Annu. Rev. Physiol.,* 1986, **48**, 657–667.

99 J. Williams, S. U. Keßel, A. C. Nölscher, Y. Yang, Y. Lee, A. M. Yáñez-Serrano, S. Wolff, J. Kesselmeier, T. Klüpfel, J. Lelieveld and M. Shao, Opposite OH reactivity and ozone cycles in the Amazon rainforest and megacity Beijing: Subversion of biospheric oxidant control by anthropogenic emissions, *Atmos. Environ.*, 2016, **125**, 112–118.

100 H. Salonen, T. Salthammer and L. Morawska, Human exposure to ozone in school and office indoor environments, *Environ. Int.*, 2018, **119**, 503–514.

101 G. Yang, Y. Liu and X. Li, Spatiotemporal distribution of ground-level ozone in China at a city level, *Sci. Rep.*, 2020, **10**, 1–12.

102 D. W. O'Sullivan, B. G. Heikes, J. Snow, P. Burrow, M. Avery, D. R. Blake, G. W. Sachse, R. W. Talbot, D. C. Thornton and A. R. Bandy, Long-term and seasonal variations in the levels of hydrogen peroxide, methylhydroperoxide, and selected compounds over the Pacific Ocean, *J. Geophys. Res. D Atmos.*, 2004, **109**, 1–21.

103 T. H. Li, B. J. Turpin, H. C. Shields and C. J. Weschler, Indoor hydrogen peroxide derived from ozone/d-limonene reactions, *Environ. Sci. Technol.*, 2002, **36**, 3295–3302.

104 Z. Zhou and J. P. D. Abbatt, Formation of Gas-Phase Hydrogen Peroxide via Multiphase Ozonolysis of Unsaturated Lipids, *Environ. Sci. Technol. Lett.*, 2021, **8(2)**, 114-120.

105 S. Zhou, Z. Liu, Z. Wang, C. J. Young, T. C. Vandenboer, B. B. Guo, J. Zhang, N. Carslaw and T. F. Kahan, Hydrogen Peroxide Emission and Fate Indoors during Non-bleach Cleaning: A Chamber and Modeling Study, *Environ. Sci. Technol.*, 2020, **54**, 15643–15651.

106 P. Artaxo, L. V. Rizzo, J. F. Brito, H. M. J. Barbosa, A. Arana, E. T. Sena, G. G. Cirino, W. Bastos, S. T. Martin and M. O. Andreae, Atmospheric aerosols in Amazonia and land use change: From natural biogenic to biomass burning conditions, *Faraday Discuss.*, 2013, **165**, 203–235.

107 N. Clements, M. P. Hannigan, S. L. Miller, J. L. Peel and J. B. Milford, Comparisons of urban and rural PM10-2.5 and PM2.5 mass concentrations and semi-volatile fractions in northeastern Colorado, *Atmos. Chem. Phys.*, 2016, **16**, 7469–7484.

108 S. Kundu, E. A. Stone, Composition and sources of fine particulate matter across urban and rural sites in the Midwestern United States. *Environ. Sci. Process Impacts*., 2014, **16**, 1360–1370.

109 S. Patel, S. Sankhyan, E. K. Boedicker, P. F. Decarlo, D. K. Farmer, A. H. Goldstein, E. F. Katz, W. W. Nazaroff, Y. Tian, J. Vanhanen and M. E. Vance, Indoor Particulate Matter during HOMEChem: Concentrations, Size Distributions, and Exposures, *Environ. Sci. Technol.*, 2020, **54**, 7107–7116.

110 A. Karambelas, T. Holloway, P. L. Kinney, A. M. Fiore, R. Defries, G. Kiesewetter, C. Heyes, Urban versus rural health impacts attributable to PM2.5 and O3 in northern India. *Environ. Res. Lett.,* 2018, **13**, 1-10.

111 T. Liu, H. Meng, M. Yu, Y. Xiao, B. Huang, L. Lin, H. Zhang, R. Hu, Z. Hou, Y. Xu, L. Yuan, M. Qin, Q. Zhao, X. Xu, W. Gong, J. Hu, J. Xiao, S. Chen, W. Zeng, X. Li, G. He, Z. Rong, C. Huang, Y. Du and W. Ma, Urban-rural disparity of the short-term association of PM2.5 with mortality and its attributable burden, *Innov.*, 2021, **2**, 100171.

112 C. S. Christensen, S. Brodsgaard, P. Mortensen, K. Egmose and S. A. Linde, Determination of hydrogen peroxide in workplace air: Interferences and method validation, *J. Environ. Monit.*, 2000, **2**, 339–343.